The Astrophysical Journal, 706:712–726, 2009 November 20 doi:10.1088/0004-637X/706/1/712

MEMORY EFFECTS IN TURBULENT TRANSPORT

Alexander Hubbard[1] and Axel Brandenburg[1,2]
[1] NORDITA, AlbaNova University Center, Roslagstullsbacken 23, SE 10691 Stockholm, Sweden; alex.i.hubbard@gmail.com
[2] Department of Astronomy, AlbaNova University Center, Stockholm University, SE 10691 Stockholm, Sweden
Received 2008 December 18; accepted 2009 October 13; published 2009 November 4

ABSTRACT

In the mean-field theory of magnetic fields, turbulent transport, i.e., the turbulent electromotive force is described by a combination of the α effect and turbulent magnetic diffusion, which are usually assumed to be proportional, respectively, to the mean field and its spatial derivatives. For a passive scalar, there is just turbulent diffusion, where the mean flux of concentration depends on the gradient of the mean concentration. However, these proportionalities are approximations that are valid only if the mean field or the mean concentration vary slowly in time. Examples are presented where turbulent transport possesses memory, i.e., where it depends crucially on the past history of the mean field. Such effects are captured by replacing turbulent transport coefficients with time integral kernels, resulting in transport coefficients that depend effectively on the frequency or the growth rate of the mean field itself. In this paper, we perform numerical experiments to find the characteristic timescale (or memory length) of this effect as well as simple analytical models of the integral kernels in the case of passive scalar concentrations and kinematic dynamos. The integral kernels can then be used to find self-consistent growth or decay rates of the mean fields. In mean-field dynamos, the growth rates and cycle periods based on steady state values of α effect, and turbulent diffusivity can be quite different from the actual values.

Key words: MHD – turbulence

1. INTRODUCTION

A simple form of turbulent transport is the mixing of a passive scalar associated with the mutual exchange of fluid parcels. This process is similar to non-turbulent mixing that occurs just because of thermal fluctuation or Brownian motion, often referred to as molecular diffusion. The latter process is described by a diffusion equation with a diffusion term of the form $\kappa\nabla^2 C$, where κ is the molecular diffusion coefficient and C is the concentration. Turbulent diffusion, on the other hand, applies to a suitably averaged mean concentration, $\overline{C}$, and is normally described by a diffusion term of the form $\kappa_t\nabla^2\overline{C}$, where κ_t is a turbulent diffusivity. The ratio κ_t/κ scales like the Reynolds number (or, more precisely, the Péclet number) and can become very large under many astrophysical conditions (stars, accretion disks, galaxies).

Problems connected with this simple prescription occur when the mean concentration shows variations on timescales shorter than or comparable to the correlation time of the turbulence. In practice, this means that a sinusoidal profile of $\overline{C}$ with wavenumber k would decay at a rate $\kappa_t k^2$, where κ_t is no longer constant, but it depends itself on the actual decay rate.

The fact that problems occur when the mean concentration changes on short timescales should not be surprising. Indeed, in the text books of Moffatt (1978) and Krause & Rädler (1980) it is shown that a proper description of turbulent transport involves a convolution of an integral kernel with the mean concentration over past times. This is why one talks about memory effects the turbulent diffusion is not just an instantaneous property of the turbulence, but depends on its full time history (Hori & Yoshida 2008). Dealing with a convolution over past times is an unpleasant complication, so its effects are often neglected. However, there can be circumstances of astrophysical relevance where this is no longer permissible.

Such a circumstance is the damping of solar p-mode oscillations through turbulent motions in the surface layers (Stix et al. 1993). Here the timescales of p-modes and convection are comparable, so memory effects must be important. Stix et al. (1993) find that the turbulent diffusion is reduced by a factor $\exp(-\omega_{\rm osc}\tau)$, where $\omega_{\rm osc}$ is the oscillation frequency, and τ is the correlation time of the turbulence. Memory effects have also been invoked in connection with propagating front solutions in the galactic dynamo (Fedotov et al. 2002, 2003), and variations of the solar cycle (Otmianowska-Mazur et al. 1997), although there the timescales are more disparate.

A practical way of dealing with memory effects has been proposed by Blackman & Field (2002, 2003), who derived an evolution equation for the turbulent flux of concentration based on a simple closure prescription known as the τ approximation. One of the main beauties of this approach is that the usual diffusion equation, which is of parabolic nature, is now replaced by a damped wave equation, which is of hyperbolic nature. This implies that signal propagation is no longer infinitely fast, but its speed is limited to the rms velocity of the turbulence. The principal validity of this approach has been demonstrated using turbulence simulations of passive scalar diffusion (Brandenburg et al. 2004). One of the goals of the present paper is to provide a more direct means of determining memory effects of turbulent transport that can also be applied to more complicated cases of vector fields such as the magnetic field.

A promising method for calculating turbulent transport coefficients for the magnetic field is the test-field method. In this approach, one calculates evolution equations for the small-scale field that results from a given set of different test fields. In this way, one can calculate the full tensorial nature of the turbulent diffusion tensor, as well as the α tensor that can be relevant for amplifying the magnetic field if the turbulence lacks mirror symmetry, for example, in the presence of helicity. These test fields have a given length scale characterized by some wavenumber. By varying this wavenumber, it has been possible to determine the scale dependence of the mean fields that are being diffused and/or amplified (Brandenburg et al. 2008a). Using a Fourier

transformation over all wavenumbers, it is possible to determine the spatial properties of the integral kernels that are used in the convolution with the mean field over all other points in space. It is customary to approximate the kernels by δ functions, in which case the convolutions become multiplications. In the test-field method, the corresponding coefficients are obtained as the limit of vanishing wavenumber. However, in order to make statements for finite domains of length L, the wavenumber $k = k_1 \equiv 2\pi/L$ is most relevant. Unless stated otherwise, we focus therefore on results for $k = k_1$.

In an analogous fashion, we can make the test fields time dependent and compute in this way the temporal properties of the integral kernels. By imposing sinusoidal variations of the test fields over a range of different frequencies, we calculate the integral kernels first in Fourier space, because there the convolution corresponds just to a multiplication. The integral kernel in real space is then obtained by Fourier transformation. Another possibility is to apply an exponentially growing or decaying time variation. In a sense this comes closest to the application of calculating modifications of growth rates due to finite memory effects. The integral kernel can then be calculated by inverse Laplace transformation, but this approach involves integration along the imaginary axis and is therefore only feasible if the data can be fitted reliably to an analytic function. We note that it is in principle also possible to determine integral kernels directly by applying a δ function-like variation to the mean concentration gradient or the mean field, but the disadvantage here is that it is then not so easy to improve the statistics by time averaging. Nevertheless, such a δ function-like perturbation provides an additional verification and is certainly a useful thought experiment.

The temporal properties of integral kernels in turbulent transport may be particularly important in dynamo theory where simulations and theory are now sufficiently accurate to show finite memory effects under controlled conditions. As a side effect, growth rates based on a dispersion relation with constant α effect and turbulent magnetic diffusivity may become inaccurate. It is quite plausible that under more complicated circumstances finite memory effects will be even more important. However, without proper knowledge of what to expect, this would only remain speculation. A goal of this paper is therefore to clarify finite memory effects in simulations of forced helical turbulence in a periodic domain. We consider here only the kinematic case, i.e., the velocity is unaffected by the magnetic field.

In Section 2, we will motivate our work by considering two approaches to calculating the growth rate of the Roberts flow dynamo. In Section 3, we define our formalism, most importantly the time response kernels that describe "memory" effects. We will treat both the turbulent transport of magnetic fields and the conceptually simpler transport of passive scalars. In Section 4, we give a brief theoretical overview before discussing our numerical simulations and results in Sections 5 and 6. We discuss those results in Section 7 and conclude in Section 8.

2. BACKGROUND: MISMATCH IN GROWTH RATES

A direct approach to determining the growth rate of a dynamo is to solve the induction equation for the magnetic field $\boldsymbol{B}$ numerically:

$$\frac{\partial \boldsymbol{B}}{\partial t} = \boldsymbol{\nabla} \times (\boldsymbol{U} \times \boldsymbol{B}) + \eta \nabla^2 \boldsymbol{B}. \quad (1)$$

Here $\boldsymbol{U}$ is the velocity and η is the microscopic magnetic diffusivity. We are interested in dynamos that produce mean fields, $\overline{\boldsymbol{B}}$, denoted here by an overbar. In the following, we take this to be an xy average. We calculate then the growth rate of the mean field as

$$\lambda_{\rm growth} = {\rm d} \ln \overline{B}_{\rm rms}/{\rm d}t. \quad (2)$$

This can now be compared with the corresponding result from mean-field theory, where one considers the averaged induction equation

$$\frac{\partial \overline{\boldsymbol{B}}}{\partial t} = \boldsymbol{\nabla} \times (\overline{\boldsymbol{U}} \times \overline{\boldsymbol{B}} + \overline{\boldsymbol{\mathcal{E}}}) + \eta \nabla^2 \overline{\boldsymbol{B}}, \quad (3)$$

with

$$\overline{\boldsymbol{\mathcal{E}}} \equiv \overline{\boldsymbol{u} \times \boldsymbol{b}} \quad (4)$$

being the turbulent electromotive force and $\boldsymbol{u} = \boldsymbol{U} - \overline{\boldsymbol{U}}$ and $\boldsymbol{b} = \boldsymbol{B} - \overline{\boldsymbol{B}}$ are the fluctuations. Symmetry considerations constrain the form of $\overline{\boldsymbol{\mathcal{E}}}$, and in the case of homogeneous isotropic turbulence with helicity, the expression for $\overline{\boldsymbol{\mathcal{E}}}$ is found to be

$$\overline{\boldsymbol{\mathcal{E}}} = \alpha \overline{\boldsymbol{B}} - \eta_{\rm t} \mu_0 \overline{\boldsymbol{J}}, \quad (5)$$

where α describes the α effect, $\eta_{\rm t}$ is the turbulent magnetic diffusivity, $\overline{\boldsymbol{J}} = \boldsymbol{\nabla} \times \overline{\boldsymbol{B}}/\mu_0$ is the mean current density, μ_0 is the vacuum permeability, and higher order terms have been omitted. Such a model is generally referred to as an α^2 dynamo. For references see Moffatt (1978) and Krause & Rädler (1980).

A new and accurate method for determining α and $\eta_{\rm t}$ is the test-field method of Schrinner et al. (2005, 2007) that will be described below. The details of this method are not essential at this point, except that we do emphasize that for our values of the magnetic Reynolds number ${\rm Re}_M$ the wavenumber of the test field is chosen to be that of the box, which is also the smallest wavenumber that fits into the domain.

For isotropic turbulence in a periodic domain, the magnetic field can develop long wavelength variations in any of the three coordinate directions (Brandenburg 2001). We assume this to be the z direction and use averages over the x and y directions. Solutions of a homogeneous α^2 dynamo obey $\boldsymbol{\nabla} \times \overline{\boldsymbol{B}} = k_z \overline{\boldsymbol{B}} = \mu_0 \overline{\boldsymbol{J}}$ and are proportional to $\exp(ik_z z + \lambda t)$ with the dispersion relation

$$\lambda = \alpha k_z - (\eta + \eta_{\rm t}) k_z^2, \quad (6)$$

where k_z is the wavenumber in the z direction. Both α and $\eta_{\rm t}$ are taken as constant in space owing to the assumed statistical homogeneity of the turbulence. For flows with positive kinetic helicity, α is expected to be negative, so growing solutions correspond to negative values of k_z.

We refer to the value of λ obtained from the dispersion relation (6) as $\lambda_{\rm disp}$. This is the second approach to determining the growth rate of the dynamo. It has the disadvantage of being indirect, but the advantage of aiding comprehension of the dynamo mechanism itself. If the theory behind this second approach is correct, then the results should match, so comparing the growth rates allows one to test the validity of Equation (5).

In order to motivate the purpose of this paper, let us now compare in Figure 1 $\lambda_{\rm growth}$ with $\lambda_{\rm disp}$ for the simpler case of a steady periodic helical flow instead of turbulence. We use here the Roberts flow, whose details will be discussed later. The two estimates for λ do indeed agree when $\lambda = 0$, at the critical magnetic Reynolds number for the onset of dynamo

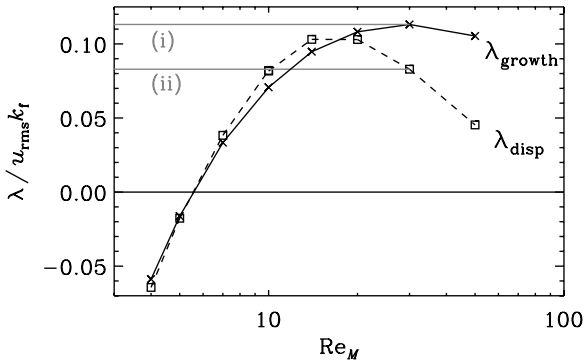

Figure 1. Re_M dependence of the growth rate for the Roberts flow as obtained from a direct calculation ($\lambda_{\rm growth}$) compared with the result of the dispersion relation, $\lambda_{\rm disp} = \alpha k_z - (\eta + \eta_{\rm t})k_z^2$, using a cubic domain of size L^3, where $k_1 = 2\pi/L$ and $k_{\rm f} = \sqrt{2}k_1$. For this range of Re_M, the most unstable mode is the largest one that fits in the box ($k_z = k_1$). The two horizontal lines in gray mark the values of $\lambda_{\rm growth}$ and $\lambda_{\rm disp}$ at $\mathrm{Re}_M = 30$, denoted by (i) and (ii), respectively.

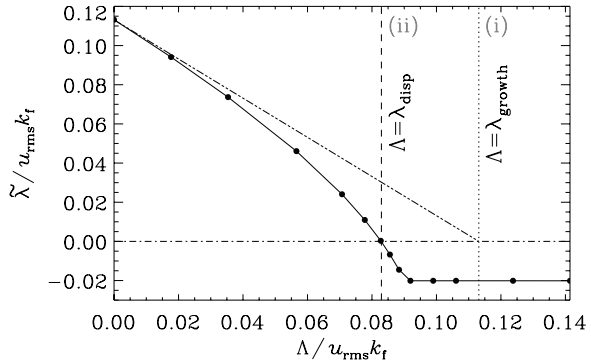

Figure 2. Dependence of $\tilde{\lambda}$ on Λ for $\mathrm{Re}_M = 30$. The values of $\Lambda = \lambda_{\rm disp}$ and $\lambda_{\rm growth}$ of Figure 1 are indicated by a vertical dashed and dotted lines, denoted by (ii) and (i), respectively. Note that $\tilde{\lambda} = 0$ (dash-dotted line) for $\Lambda = \lambda_{\rm disp}$, where $\lambda_{\rm disp} = \alpha k_z - (\eta + \eta_{\rm t})k_z^2$, with α and $\eta_{\rm t}$ obtained using the test-field method for steady fields. The linear interpolation between the points $(\Lambda, \tilde{\lambda}) = (0, \lambda_{\rm growth})$ and $(\lambda_{\rm growth}, 0)$ is indicated by a triple-dot-dash line.

action $\mathrm{Re}_{M,\rm crit} \simeq 5.52$. For larger values of Re_M, there is a discrepancy that can become rather dramatic for $\mathrm{Re}_M > 20$.

One of the motivations for our work then is the fact that the growth rate estimated from Equation (6), where α and $\eta_{\rm t}$ are obtained from the test-field method, becomes increasingly inaccurate for large growth rates, implying that Equation (5) is inadequate to describe growing dynamos. We emphasize that this discrepancy vanishes not only in the marginal case, but also for the nonlinearly saturated dynamo. This is why in Brandenburg et al. (2008b) the quenched values of $\alpha(\overline{\boldsymbol{B}})$ and $\eta_{\rm t}(\overline{\boldsymbol{B}})$ were found to obey Equation (6) with $\lambda = 0$.

Even though the Roberts flow has been studied extensively over the years (see, e.g., Roberts 1972; Soward 1987; Plunian et al. 1999; Plunian & Rädler 2002a, 2002b; Courvoisier 2008), and especially so in connection with the Karlsruhe dynamo experiment (cf. Stieglitz & Müller 2001; Rädler et al. 2002), a discrepancy between theoretically expected growth rates based on mean-field theory and the actual ones has never been reported. For example, in Plunian & Rädler (2002a), the actual growth rates have been determined directly without invoking mean-field theory, and in Rädler et al. (2002) only the marginal case has been compared with observations. However, in the marginal case the discrepancy disappears. In Plunian & Rädler (2002b), on the other hand, the values of α and $\eta_{\rm t}$ have again been determined self-consistently for cases different from the marginal one. Thus, the mean field is then of course no longer steady, and so their values of α and $\eta_{\rm t}$ apply only to this particular time dependence, but not to a fictitious steady case, for example. We say here "fictitious," because for given values of Re_M and k_z, there is normally only one relevant solution, namely the one with the largest value of λ. However, for a predictive theory, one should know α and $\eta_{\rm t}$ before having solved the problem, i.e., before knowing λ. In the following, we explain how the fictitious steady case can actually be realized in a simulation.

In order to clarify the point that, for given values of Re_M, α and $\eta_{\rm t}$ depend also on the resulting growth rate, let us now consider a modified induction equation with an artificial "friction" term

$$\frac{\partial \boldsymbol{B}}{\partial t} = \boldsymbol{\nabla} \times (\boldsymbol{U} \times \boldsymbol{B}) + \eta \nabla^2 \boldsymbol{B} - \Lambda \overline{\boldsymbol{B}}, \tag{7}$$

where Λ is a new control parameter and $\overline{\boldsymbol{B}}$ is the xy-averaged field. Note that the evolution of the departure from this xy-averaged field, $\boldsymbol{b} = \boldsymbol{B} - \overline{\boldsymbol{B}}$, is unaffected by this manipulation, so $\overline{\boldsymbol{\mathcal{E}}} = \overline{\boldsymbol{u} \times \boldsymbol{b}}$ is exactly the same as before. The solutions of $\boldsymbol{B}$ have still an exponential time dependence, and standard mean-field theory gives for the growth rate $\tilde{\lambda}$of the mean field

$$\tilde{\lambda} = \alpha k_z - (\eta + \eta_{\rm t})k_z^2 - \Lambda. \tag{8}$$

So, as the value of Λ is increased (for given values of Re_M and k_z), the growth rate $\tilde{\lambda}$ decreases. (The tilde has been added to distinguish λ from that used in Equation (6).) There is a critical value Λ_* for which $\tilde{\lambda} = 0$. This value is determined by

$$\Lambda_* = \alpha k_z - (\eta + \eta_{\rm t})k_z^2. \tag{9}$$

Given that in this case the mean field is steady, we now expect Equation (9) to be accurate. To verify this, we solve Equation (7) numerically and determine the growth rate $\tilde{\lambda}$. The result is shown in Figure 2 where we plot $\tilde{\lambda}$ versus Λ for $\mathrm{Re}_M = 30$. For $\Lambda = 0$, we find $\tilde{\lambda} = \lambda_{\rm growth}$. More importantly, it turns out that $\tilde{\lambda} = 0$ at a value $\Lambda = \Lambda_* = \lambda_{\rm disp}$, indicated by (ii), that is given by Equation (9) with the same values of α and $\eta_{\rm t}$ that led earlier to the discrepancy in Figure 1. Most crucially, the numerically determined growth rate $\tilde{\lambda}$ in Figure 2 deviates from a linear interpolation between the points $(\Lambda, \tilde{\lambda}) = (0, \lambda_{\rm growth})$ and $(\lambda_{\rm growth}, 0)$. This suggests again that the assumption of the α and $\eta_{\rm t}$in Equation (8) being independent of λ is invalid.

We note that for larger values of Re_M (e.g., for $\mathrm{Re}_M = 50$), Equation (7) permits additional solutions with insignificant $\overline{\boldsymbol{B}}$ that cannot be damped by the $\Lambda\overline{\boldsymbol{B}}$ term. However, as a proof of concept, it was only essential that Re_M was big enough so that there is a clear difference between $\lambda_{\rm growth}$ and $\lambda_{\rm disp}$.

The results presented above show that a naive application of the dispersion relation to cases where $\lambda \neq 0$ is not possible and gives results that disagree with the direct simulation. This is because the values of α and $\eta_{\rm t}$ apply only to the steady case, as demonstrated by considering the associated steady problem of Equation (7), where $\Lambda = \Lambda_*$ is predicted from Equation (9) using the α and $\eta_{\rm t}$ values obtained from the test-field method.

Recently, Hori & Yoshida (2008) noted that, in the Roberts flow, memory effects can be responsible for an enhancement of the growth rate. The reason why Plunian & Rädler (2002b) found the correct growth rates from Equation (6) even when $\lambda \neq 0$ is

that their values of α and η_t were automatically "tuned" to the resulting growth rate. Their values do therefore not apply to the steady case, which can be verified by considering the mean-field problem associated with Equation (7).

To understand the reason for the discrepancy between actual growth rates and those obtained from the standard (time-independent) test-field method, it is important to recall that a multiplicative relation in Equation (5) is only an approximation and that it should instead be a convolution in space and time (Moffatt 1978; Krause & Rädler 1980). Alternatively, a Taylor series expansion of $\overline{\boldsymbol{\mathcal{E}}}$ in space and time can be employed. Already in the simple case of the Roberts flow Equation (5) cannot be justified when the mean field changes sufficiently rapidly in time. In this paper, we show that in such cases "memory" effects of the turbulent transport coefficients cannot be ignored. This implies that the electromotive force at a given time depends not only on the mean fields at that specific time, but also on the mean fields at all prior times. In practice, this means that the turbulent transport coefficients depend themselves on the resulting growth rate and/or frequency of the mean fields.

3. FORMALISM

Quite generally, we are interested in expressing quadratic correlations of fluctuating quantities in terms of mean fields. Examples include the mean turbulent concentration flux and the mean turbulent electromotive force,

$$\overline{\boldsymbol{\mathcal{F}}} = \overline{\boldsymbol{u}c}, \quad \text{and} \quad \overline{\boldsymbol{\mathcal{E}}} = \overline{\boldsymbol{u}\times\boldsymbol{b}}, \tag{10}$$

respectively. Here, $c = C - \overline{C}$ is the fluctuation of the concentration density. The number of preferred directions available to mean quantities such as $\overline{\boldsymbol{\mathcal{F}}}$ and $\overline{\boldsymbol{\mathcal{E}}}$ are limited, and so the aim is to relate them respectively to the gradient of the mean concentration, $\overline{\boldsymbol{G}} = \boldsymbol{\nabla}\overline{C}$, and to a linear combination of the mean magnetic field $\overline{\boldsymbol{B}}$ and its curl, $\boldsymbol{\nabla}\times\overline{\boldsymbol{B}} = \mu_0\overline{\boldsymbol{J}}$. However, instead of multiplicative (instantaneous) relations of the form

$$\overline{\boldsymbol{\mathcal{F}}} = -\kappa_t\overline{\boldsymbol{G}}, \qquad \overline{\boldsymbol{\mathcal{E}}} = \alpha\overline{\boldsymbol{B}} - \eta_t\mu_0\overline{\boldsymbol{J}}, \tag{11}$$

we now adopt such relations in their more general forms involving a convolution in time, i.e.,

$$\overline{\boldsymbol{\mathcal{F}}}(t) = -\int_{-\infty}^{t}\hat{\kappa}_t(t-t')\overline{\boldsymbol{G}}(t')\,\mathrm{d}t', \tag{12}$$

and

$$\overline{\boldsymbol{\mathcal{E}}}(t) = \int_{-\infty}^{t}\hat{\alpha}(t-t')\overline{\boldsymbol{B}}(t')\,\mathrm{d}t' - \int_{-\infty}^{t}\hat{\eta}_t(t-t')\mu_0\overline{\boldsymbol{J}}(t')\,\mathrm{d}t', \tag{13}$$

where quantities with a hat denote integral kernels, so $\hat{\kappa}_t(t)$ is an integral kernel describing turbulent passive scalar diffusion, $\hat{\alpha}(t)$ describes the α effect, and $\hat{\eta}_t(t)$ the turbulent magnetic diffusion. This approach is the most general search for memory effects, and we adopt it to find out how to modify Equation (5) to model more accurately growing dynamos.

We recall that in general our averages (being two dimensional over the xy plane) are also functions of z, but the z dependence has here been suppressed in favor of a more compact notation. In general, Equations (12) and (13) should also include a convolution over z. This property has recently been studied in Brandenburg et al. (2008a), but the spatial aspects of the convolution will here be ignored by considering magnetic fields that have only a single wavenumber k_z, which corresponds to the smallest wavenumber $k_1 = 2\pi/L$ that fits into the domain of size L^3.

3.1. Standard Test-field Methods

In this section, we reiterate the essence of the standard test-field methods for calculating α, η_t, and κ_t, where memory effects are ignored. As noted above, mean-field theory treats turbulent transport through the correlations of fluctuating quantities as in Equation (11). If the transported quantity does not itself affect the dynamics of the system, as in the cases of passive scalars or kinematic dynamos (where the magnetic field is too weak to affect the momentum equation), then the transport coefficients are functions of the velocity fields alone.

This lack of dependence of the transport coefficients on the mean field implies that the transport coefficients will be found also in systems where a mean field is externally imposed and does not obey any evolution equation. Such a field is called a test field. A set of different test fields is needed to determine simultaneously the prefactors α and η_t of $\overline{\boldsymbol{B}}$ and $\overline{\boldsymbol{J}}$, respectively. In the test-field method of Schrinner et al. (2005, 2007), one subtracts the mean-field Equation (3) from the full induction Equation (1) to obtain an evolution equation for the fluctuating field $\boldsymbol{b}$,

$$\frac{\partial\boldsymbol{b}}{\partial t} = \boldsymbol{\nabla}\times(\overline{\boldsymbol{U}}\times\boldsymbol{b} + \boldsymbol{u}\times\overline{\boldsymbol{B}} + \boldsymbol{u}\times\boldsymbol{b} - \overline{\boldsymbol{u}\times\boldsymbol{b}}) + \eta\nabla^2\boldsymbol{b}. \tag{14}$$

This equation is then applied separately to each of the fields $\overline{\boldsymbol{B}}^{pq}$, where $p = 1$ or 2 and $q = c$ or s label different test fields. Brandenburg et al. (2008a, 2008b) use the four test fields

$$\overline{\boldsymbol{B}}^{1ck} = B_0(\cos kz, 0, 0), \qquad \overline{\boldsymbol{B}}^{1sk} = B_0(\sin kz, 0, 0), \tag{15}$$

$$\overline{\boldsymbol{B}}^{2ck} = B_0(0, \cos kz, 0), \qquad \overline{\boldsymbol{B}}^{2sk} = B_0(0, \sin kz, 0), \tag{16}$$

where the third superscript k has been added to denote the wavenumber, and B_0 is a normalization factor. The response to each test field, $\boldsymbol{b}^{pqk}$, is found by solving Equation (14). In this way, one finds $\overline{\boldsymbol{\mathcal{E}}}^{pqk} = \overline{\boldsymbol{u}\times\boldsymbol{b}^{pqk}}$ and obtains 4×2 equations,

$$\overline{\mathcal{E}}_i^{pqk} = \alpha_{ij}\overline{B}_j^{pqk} - \eta_{ij}\mu_0\overline{J}_j^{pqk}, \tag{17}$$

for the $4+4$ unknowns, α_{ij} and η_{ij}, for $i = 1, 2$ and $j = 1, 2$. These eight unknowns are obtained as

$$\begin{pmatrix}\alpha_{ij}\\ \eta_{ij3}k\end{pmatrix} = B_0^{-1}\begin{pmatrix}\cos kz & \sin kz\\ -\sin kz & \cos kz\end{pmatrix}\begin{pmatrix}\overline{\mathcal{E}}_i^{jck}\\ \overline{\mathcal{E}}_i^{jsk}\end{pmatrix}, \tag{18}$$

where the rank-3 tensor η_{ij3} is related to the rank-2 tensor in Equation (17) via $\eta_{ij} = \eta_{ik3}\epsilon_{jk3}$. Note that the result is independent of the value of B_0. For stationary isotropic homogeneous turbulence, we have constant values of $\alpha_{11} = \alpha_{22} \equiv \alpha$ and $\eta_{11} = \eta_{22} \equiv \eta_t$, except for statistical fluctuations resulting from finite computational volumes.

The test-field method for a passive scalar works analogously (Brandenburg et al. 2009). The concentration per unit volume C obeys the equation

$$\frac{\partial C}{\partial t} = -\boldsymbol{\nabla}\cdot(\boldsymbol{U}C) + \kappa\nabla^2 C, \tag{19}$$

and the evolution of the mean concentration $\overline{C}$ is obtained by averaging Equation (19), which yields

$$\frac{\partial \overline{C}}{\partial t} = -\boldsymbol{\nabla} \cdot (\overline{\boldsymbol{U}}\,\overline{C} + \overline{\boldsymbol{\mathcal{F}}}) + \kappa \nabla^2 \overline{C}. \tag{20}$$

The test-scalar equation is obtained by subtracting Equation (20) from Equation (19), which yields

$$\frac{\partial c}{\partial t} = -\boldsymbol{\nabla} \cdot (\overline{\boldsymbol{U}} c + \boldsymbol{u}\overline{C} + \boldsymbol{u}c - \overline{\boldsymbol{u}c}) + \kappa \nabla^2 c. \tag{21}$$

In order to obtain κ_t, one uses the test scalars

$$\overline{C}^{ck} = C_0 \cos kz, \qquad \overline{C}^{sk} = C_0 \sin kz, \tag{22}$$

where $q = c$ or s denotes the spatial dependence of the test scalar and, again, an additional superscript k denotes the wavenumber, while C_0 is a normalization factor. For each test scalar, we obtain a separate evolution equation for c^{qk}. In this way, we calculate the fluxes, $\overline{\boldsymbol{\mathcal{F}}}^{qk} = \overline{\boldsymbol{u}c^{qk}}$, and compute the three components of κ_{i3}:

$$\kappa_{i3} = -\left\langle -\sin kz\,\overline{\mathcal{F}}_i^{ck} + \cos kz\,\overline{\mathcal{F}}_i^{sk} \right\rangle_z \Big/ kC_0, \tag{23}$$

for $i = 1, \ldots, 3$, where $\langle\,\rangle_z$ denotes a z average. Again, the values of κ_{i3} are independent of the normalization constant C_0. For stationary isotropic homogeneous turbulence, we have, except for statistical fluctuations, constant $\kappa_{ij} = \kappa_t \delta_{ij}$.

By applying the test-field and test-scalar methods to a range of different wavenumbers k, it was possible to assemble two full integral kernels in space (Brandenburg et al. 2008b, 2009) and hence to take the effects of finite scale separation into account. In the following, we proceed analogously by applying the test-field and test-scalar methods to a range of different frequencies to assemble two full integral kernels in time and hence to take memory effects into account.

3.2. Determination of the Kernels

As is common in linear response theory, all integral kernels vanish for $t < 0$. Therefore, the integrations in Equations (12) and (13) extend effectively only to $t' = t$. In order to determine these kernels numerically, we can either calculate them directly by imposing δ function-like variations of the test fields, or we can use the fact that a convolution corresponds to a multiplication in spectral space, i.e.,

$$\tilde{\boldsymbol{\mathcal{F}}}(\omega) = -\tilde{\kappa}_t(\omega)\tilde{\boldsymbol{G}}(\omega), \tag{24}$$

where

$$\tilde{\kappa}_t(\omega) = \int \mathrm{d}t\, e^{i\omega t} \hat{\kappa}_t(t) \tag{25}$$

is the Fourier transform of $\hat{\kappa}_t(t)$.

A multiplicative relation between $\overline{\boldsymbol{\mathcal{F}}}$ and $\overline{\boldsymbol{G}}$ applies also to the Laplace transform of these functions with

$$\tilde{\boldsymbol{\mathcal{F}}}(s) = -\tilde{\kappa}_t(s)\tilde{\boldsymbol{G}}(s), \tag{26}$$

where

$$\tilde{\kappa}_t(s) = \int_0^\infty \mathrm{d}t\, e^{-st} \hat{\kappa}_t(t) \tag{27}$$

is now the Laplace transformation of $\hat{\kappa}_t(t)$.

We introduce an additional superscript ω for the cases where the test fields or concentrations have $\cos \omega t$ time dependence and superscript s for the cases where the test fields or concentrations have $\exp st$ time dependence. The superscripts or the explicit time dependence are sometimes suppressed. In most of the cases, we use test fields with a sinusoidal spatial dependence with wavenumber $k = k_1$. However, it is sometimes useful to vary also the value of k. In these cases, we also add the superscript k.

The multiplicative relations above imply that for an oscillatory perturbation with a single frequency there is a multiplicative relation between $\overline{\boldsymbol{G}}^{qk\omega}(t)$ and $\overline{\boldsymbol{\mathcal{F}}}^{qk\omega}(t)$, where the first superscript denotes the frequency; see Appendix A. In general, κ_t is a tensor, but in the following, we restrict ourselves to determining only one of its components, namely the one relating the z components of $\overline{\boldsymbol{\mathcal{F}}}(t)$ and $\overline{\boldsymbol{G}}(t)$ to each other. We therefore assume $\overline{\boldsymbol{G}}(z, t) = (0, 0, \overline{G})$, where $\overline{G} = \partial C/\partial z$. The different test scalars $C^{qk\omega}$ are denoted by superscripts c and s for spatial dependences proportional to $\cos kz$ and $\sin kz$, so we have

$$\overline{C}^{ck\omega} = C_0 \cos kz \cos \omega t, \quad \overline{C}^{sk\omega} = C_0 \sin kz \cos \omega t, \tag{28}$$

for oscillatory test fields, and

$$\overline{C}^{cks} = C_0 \cos kz \exp st, \quad \overline{C}^{sks} = C_0 \sin kz \exp st, \tag{29}$$

for exponentially growing or decaying test fields. For each value of ω, we determine the resulting z component of the flux, $\overline{\mathcal{F}}_\omega(t)$. As shown in Equation (A4) of Appendix A, we can calculate the response kernel as

$$\tilde{\kappa}_t(k, \omega) = -2G_0^{-1} \langle e^{i\omega t} \overline{\mathcal{F}}^{k\omega}(t) \rangle_t, \tag{30}$$

where the subscript t behind an angular bracket denotes a time average. Note that $\tilde{\kappa}_t(k, \omega)$ is complex such that its real part is symmetric about $\omega = 0$, while the imaginary part is antisymmetric. In other words, it obeys the Kramers relation, $\tilde{\kappa}_t(k, -\omega) = \tilde{\kappa}_t{}^*(k, \omega)$, where the asterisk denotes the complex conjugation; see, e.g., Moffatt (1978) and Krause & Rädler (1980). In our case, in addition, $\tilde{\kappa}_t$ is symmetric in k.

Analogous relations apply to $\tilde{\boldsymbol{\mathcal{F}}}(s)$ and $\tilde{\boldsymbol{G}}(s)$. In this case, Equation (30) is modified to

$$\tilde{\kappa}_t(k, s) = -G_0^{-1} \langle e^{-st} \overline{\mathcal{F}}^{ks}(t) \rangle_t. \tag{31}$$

As discussed in Section 3.1, our test fields allow us to pick out each tensor component of α_{ij} and η_{ij} separately. We therefore define time-dependent test fields

$$\overline{\boldsymbol{B}}^{pqk\omega} = \overline{\boldsymbol{B}}^{pqk} \cos \omega t, \quad \text{and} \quad \overline{\boldsymbol{B}}^{pqks} = \overline{\boldsymbol{B}}^{pqk} \exp st, \tag{32}$$

where the time-independent test fields $\overline{\boldsymbol{B}}^{pqk}$ were defined in Equation (17). Owing to variations of the form $\sin kz$ and $\cos kz$ one multiplies with the inverse of a rotation matrix

$$\begin{pmatrix} \tilde{\alpha}_{ij}(k, s) \\ \tilde{\eta}_{ij3}(k, s)k \end{pmatrix} = \left\langle e^{-st} \begin{pmatrix} \cos kz & \sin kz \\ -\sin kz & \cos kz \end{pmatrix} \begin{pmatrix} \overline{\mathcal{E}}_i^{1jks} \\ \overline{\mathcal{E}}_i^{2jks} \end{pmatrix} \right\rangle_t, \tag{33}$$

where the matrix above results from the choice of the sinusoidal test fields; see Sur et al. (2008) for details. An analogous equation applies also to the case of oscillatory test fields where s is replaced by $-i\omega$, so we write

$$\begin{pmatrix} \tilde{\alpha}_{ij}(k, \omega) \\ \tilde{\eta}_{ij3}(k, \omega)k \end{pmatrix} = \left\langle e^{i\omega t} \begin{pmatrix} \cos kz & \sin kz \\ -\sin kz & \cos kz \end{pmatrix} \begin{pmatrix} \overline{\mathcal{E}}_i^{1jk\omega} \\ \overline{\mathcal{E}}_i^{2jk\omega} \end{pmatrix} \right\rangle_t, \tag{34}$$

keeping in mind that a tilde has been used to indicate both Fourier and Laplace transformation.

4. PRELIMINARY CONSIDERATIONS

Before entering the numerical determination of the integral kernels let us consider a current approach that captures memory effects, as well as its simplest extension. This will later serve us with a useful fit formula for the more complicated cases.

4.1. Expectations from the τ Approximation

We use the term τ approximation here in the form introduced by Blackman & Field (2002, 2003, 2004). The essence of the τ approximation is to write down evolution equations for second-order correlations such as $\overline{\boldsymbol{u}c}$ and $\overline{\boldsymbol{u}\times\boldsymbol{b}}$. This results in triple correlations that are not omitted, as in the first-order smoothing approximation (FOSA), but are instead approximated by a closure hypothesis. In the τ approximation, one replaces the triple correlations by quadratic correlations divided by a relaxation time τ (Vainshtein & Kitchatinov 1983; Kleeorin et al. 1996). This timescale is expected to be comparable to the turnover time of the turbulence.

Blackman & Field (2002, 2003, 2004) were the first to *retain* the time derivative in the evolution equations for $\overline{\boldsymbol{u}c}$ and $\overline{\boldsymbol{u}\times\boldsymbol{b}}$. This means that the Fickian diffusion approximation of Equation (11), i.e., $\overline{\boldsymbol{\mathcal{F}}} = -\tilde{\kappa_{\rm t0}}\overline{\boldsymbol{G}}$, with $\tilde{\kappa_{\rm t0}} = \tau\overline{u_z^2}$ for one-dimensional diffusion in the z direction, is generalized to

$$\left(1+\tau\frac{\partial}{\partial t}\right)\overline{\boldsymbol{\mathcal{F}}} = -\tilde{\kappa_{\rm t0}}\overline{\boldsymbol{G}}. \tag{35}$$

This implies that the Fourier-transformed integral kernel is

$$\tilde{\kappa_{\rm t}}(\omega) = \frac{\tilde{\kappa_{\rm t0}}}{1-i\omega\tau} = \frac{\tau\overline{u_z^2}}{1-i\omega\tau}. \tag{36}$$

(Any k dependence is here ignored.) In real space, this expression for $\tilde{\kappa_{\rm t}}(\omega)$ corresponds to the integral kernel

$$\hat{\kappa_{\rm t}}(t) = \int_{-\infty}^{\infty}\frac{{\rm d}\omega}{2\pi}e^{-i\omega t}\frac{\tau\overline{u_z^2}}{1-i\omega\tau} = \overline{u_z^2}\,\Theta(t)\,e^{-t/\tau}, \tag{37}$$

where the integral has been solved as a contour integral around the pole at $\omega = -i/\tau$, and Θ is the Heaviside step function with $\Theta(t) = 1$ for $t > 0$ and 0 otherwise. In the limit $\tau \to 0$, the exponential function reduces to $\tau\delta(t)$, so

$$\hat{\kappa_{\rm t}}(t) \to \tau\overline{u_z^2}\,\delta(t) = \tilde{\kappa_{\rm t0}}\delta(t) \quad (\text{for } \tau\to 0), \tag{38}$$

and one recovers the usual prediction in which turbulent diffusion can be treated as a multiplicative enhanced diffusion coefficient.

Similar considerations also apply to the case with magnetic fields, where $\overline{\boldsymbol{\mathcal{E}}}$ is essentially being replaced by $(1+\tau\partial_t)\overline{\boldsymbol{\mathcal{E}}}$. For exponentially growing solutions, one would therefore expect that the actual growth rate λ is reduced by a factor $(1+\lambda\tau)^{-1}$. However, this expectation may be too naive and will need to be reconsidered in this work.

A useful diagnostic for the applicability of Equation (36) is that the value of ω where ${\rm Re}\,\kappa_{\rm t} = {\rm Im}\,\kappa_{\rm t}$ is also the value of ω where ${\rm d\,Im}\,\kappa_{\rm t}/{\rm d}\omega = 0$ (i.e., where the phase is $\pi/4$, see Figure 3, final panel). It will turn out that this property is not always obeyed.

4.2. Effects Beyond FOSA and τ Approximation

While a δ function perturbation is disadvantageous numerically, it can be illuminating. If we impose a test-field $\overline{C}$ with a $\delta(t)$ time dependence on a flow with $\overline{\boldsymbol{U}} = \boldsymbol{0}$, then the value of $c(0)$ depends only on the $\boldsymbol{\nabla}\cdot(\boldsymbol{u}\overline{C})$ term in Equation (21). For $t > 0$, Equation (21) reduces then to

$$\frac{\partial c}{\partial t} = -\boldsymbol{\nabla}\cdot(\boldsymbol{u}c - \overline{\boldsymbol{u}c}) + \kappa\nabla^2 c \quad (t>0). \tag{39}$$

Such a δ perturbation then launches fluctuating fields which evolve according to an equation similar to Equation (39). In passive scalar or kinematic dynamo cases, the evolution of the fluctuating field depends only on $\boldsymbol{u}$, which is independent of the fluctuating field. The fluctuating fields will decay exponentially according to turbulent or micro-physical diffusion or resistivity, but they will generate $\overline{\boldsymbol{\mathcal{F}}}$ (or $\overline{\boldsymbol{\mathcal{E}}}$ in the magnetic case) for as long as they survive. It is the finite lifetime of the fluctuating fields that is at the physical core of this memory effect.

In the passive scalar case, we consider $\overline{\boldsymbol{\mathcal{F}}} = \overline{\boldsymbol{u}c}$ to which the term $\boldsymbol{\nabla}\cdot(\overline{\boldsymbol{u}c})$ in Equation (39) does not contribute because $\overline{\boldsymbol{u}\boldsymbol{\nabla}\cdot(\overline{\boldsymbol{u}c})} = 0$. If the spatial dependence of our test scalar $\overline{C}$ is sinusoidal and lies only along a direction $\hat{z}$, then $c(0)$ will also have only sinusoidal behavior in that direction. If we imagine that the initial $c(0)$ is proportional to $\sin kz$, then, in the absence of other effects, two counter-propagating vertical streams with $u_z = \pm u$ (assuming $\overline{\boldsymbol{U}} = 0$) will generate an advective sinusoidal signal from the $\nabla_z(u_z c)$ term of Equation (39):

$$\overline{u_z\nabla_z(u_z c)}(t,z) = 2u^2 k\cos kz\cos\omega_0 t, \tag{40}$$

where $\omega_0 = ku$. In a turbulent system, the above analysis can only be done for times shorter than or comparable to a turbulent correlation time $\tau \sim 1/ku$. For times larger than a turbulent correlation time, the standard $e^{-t/\tau}$ diffusion term will be important. A "turbulent" diffusion is formally possible even in steady flows, but it will be just the microscopic diffusion.

We can combine the short timescale advective (oscillatory) and longer timescale diffusive (exponential) effects by a simple multiplication: we expect the form for $\hat{\kappa_{\rm t}}(t)$ to be similar to

$$\hat{\kappa_{\rm t}}(t) \simeq u^2\,\Theta(t)\,e^{-t/\tau}\cos\omega_0 t. \tag{41}$$

Note that in a turbulent system we expect $\omega_0 \sim 1/\tau$ on dimensional grounds and so the above analysis is not rigorous. However, as we will see in Section 6 this form fits the results reasonably well. In the Fourier space this becomes

$$\frac{\tilde{\kappa_{\rm t}}(\omega)}{\tilde{\kappa_{t0}}} = \frac{1-i\omega\tau}{(1-i\omega\tau)^2+\omega_0^2\tau^2}, \tag{42}$$

where $\tilde{\kappa_{t0}} = \tau u^2$ has been assumed, although this prefactor may not be accurate for $\omega_0 \neq 0$. The corresponding Laplace transform is

$$\frac{\tilde{\kappa_{\rm t}}(s)}{\tilde{\kappa_{t0}}} = \frac{1+s\tau}{(1+s\tau)^2+\omega_0^2\tau^2}. \tag{43}$$

In the limit $\omega_0 \to 0$, these expressions coincide with those of Section 4.1. In Figure 3, we plot various representations of the integral kernel for different values of $\omega_0\tau$.

In order to assess whether the proposed extension to capturing memory effects is viable, we shall use Equations (42) and (43)

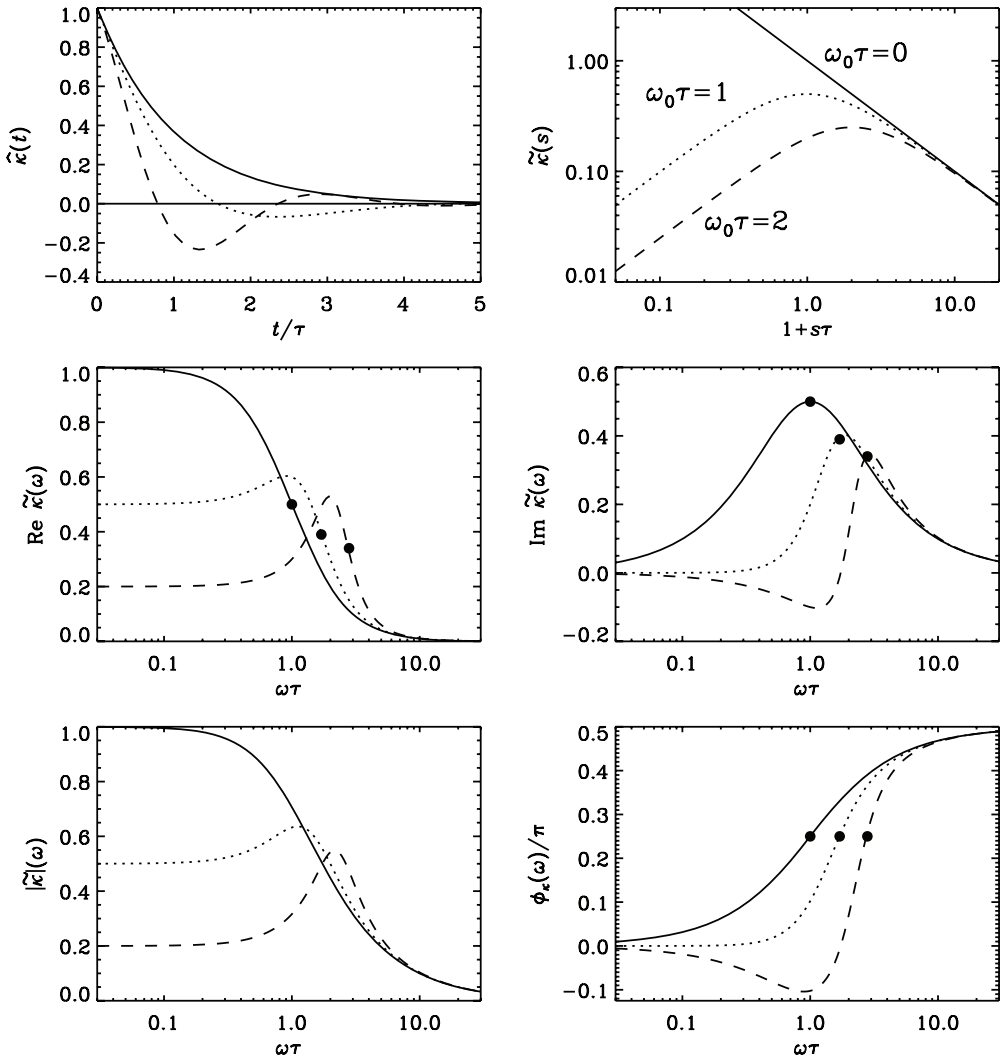

Figure 3. Plots of the model integral kernel given by Equation (41) for $\omega_0\tau = 0$ (solid lines), 1 (dotted lines), and 2 (dashed lines), compared with its Laplace transform ($\tilde{\kappa}_t(s)$), the real and imaginary parts of $\tilde{\kappa}_t(\omega)$, its modulus $|\tilde{\kappa}_t|$, and phase ϕ_κ. The positions where $\mathrm{Re}\,\kappa_t = \mathrm{Im}\,\kappa_t$ are marked with filled symbols in three relevant panels.

as fit formulae to determine the value of ω_0 and to find out how it depends on other aspects of the model such as the Péclet number and wavenumber of the mean concentration.

In the absence of a detailed analogous motivation for α and η_t, we shall use in this paper Equations (42) and (43) as fit formulae also in the magnetic case. In this case, we use these formulae for α and η_t and add corresponding subscripts α and η to τ and ω_0, where it replaces the subscript 0, i.e., we write

$$\frac{\tilde{\alpha}(\omega)}{\tilde{\alpha}_0} = A_\alpha \frac{1 - i\omega\tau_\alpha}{(1 - i\omega\tau_\alpha)^2 + \omega_\alpha^2\tau_\alpha^2}, \tag{44}$$

$$\frac{\tilde{\eta}_t(\omega)}{\tilde{\eta}_{t0}} = A_\eta \frac{1 - i\omega\tau_\eta}{(1 - i\omega\tau_\eta)^2 + \omega_\eta^2\tau_\eta^2}. \tag{45}$$

Again, we expect $\omega_\alpha\tau_\alpha$ and $\omega_\eta\tau_\eta$to be of order unity, but in this paper we allow them to be adjustable parameters. Further, we use A_α and A_η as further fit parameters, modifying the amplitude. The relaxation times τ and ω_0^{-1} and values derived from them such as $\tilde{\alpha}_{t0}$ are merely characteristic times, and we do not attempt to laboriously average over the true values.

Note that the above form for the kernel, Equation (41), is the simplest extension of the τ approximation that qualitatively fits our simulation results. From that perspective, we replace Equation (35) by

$$\left(1 + \omega_0^2\tau^2 + 2\tau\frac{\partial}{\partial t} + \tau^2\frac{\partial^2}{\partial t^2}\right)\overline{\mathcal{F}} = -\tilde{\kappa}_t\left(1 + \tau\frac{\partial}{\partial t}\right)\overline{\boldsymbol{G}}. \tag{46}$$

Note also that, unlike Equation (36), for Equation (42), the value of ω where the slope of the imaginary component is zero is not the same as the value of ω where the phase is $\pi/4$ (see the end of Section 4.1).

As shown in Equation (A5) of Appendix A, for monochromatic mean fields a phase shift ϕ_κ leads to a time lag

$$\Delta t = \phi_\kappa(\omega)/\omega, \tag{47}$$

so the flux $\overline{\mathcal{F}}_\omega(t)$ depends only on the mean concentration gradient at time $t - \Delta t$ and is given by $-|\tilde{\kappa}|\,\overline{G}(t - \Delta t)$. For the response function given by Equation (42), the time lag is

$$\frac{\Delta t}{\tau} = \frac{\phi_\kappa(\omega)}{\omega\tau} = \frac{1}{\omega\tau}\arctan\left[\omega\tau\frac{1 + \left(\omega^2 - \omega_0^2\right)\tau^2}{1 + \left(\omega^2 + \omega_0^2\right)\tau^2}\right], \tag{48}$$

which always vanishes for large values of ω and can have a peak near $\omega\tau = 1$ for $\omega_0 > \omega_0^*$with $\omega_0^*\tau \approx 0.3273$; see Figure 4.

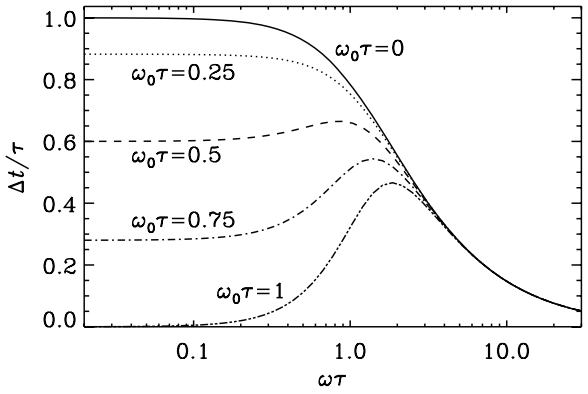

Figure 4. Normalized time lag $\Delta t/\tau$ vs. $\omega\tau$ for different values of $\omega_0\tau$. Note the development of a peak near $\omega\tau = 1$ as $\omega_0\tau$ is increased.

5. SIMULATIONS

We consider two types of flows. For test purposes and comparison with earlier work described in Section 2, we use the Roberts flow. The Roberts flow is given by

$$\boldsymbol{U} = k_{\rm f}\psi\hat{\boldsymbol{z}} - \hat{\boldsymbol{z}}\times\boldsymbol{\nabla}\psi, \tag{49}$$

with

$$\psi = (u_0/k_0)\cos k_0 x \cos k_0 y \tag{50}$$

and $k_{\rm f} \equiv \sqrt{2}k_0$ so that $k_{\rm f}^2 = k_x^2 + k_y^2$, where $k_x = k_y = k_0$ is the wavenumber of the flow in the x–y plane. This flow is capable of dynamo action once the magnetic Reynolds number

$$\mathrm{Re}_M = u_{\rm rms}/\eta k_0, \tag{51}$$

exceeds a critical value, $\mathrm{Re}_M \geqslant \mathrm{Re}_{M,\rm crit} \equiv 5.52$. We recall that our test fields have spatial dependence given by k_1, i.e., the smallest wavenumber that fits in the box. We note further that for $\mathrm{Re}_M \leqslant 70$ the most unstable wavenumber of the field that fits into the box is still $|k_z| = k_1$, where k_z was defined in Equation (6) and this agrees with the wavenumber of the test fields. Note, however, that, for $\mathrm{Re}_M = 100$, for example, the most unstable mode would have $|k_z| = 2k_1$.

The other alternative is forced turbulence. In this case, we consider an isothermal equation of state with a constant sound speed, $c_{\rm s}$, and solve the momentum and continuity equations

$$\frac{\partial \boldsymbol{U}}{\partial t} = -\boldsymbol{U}\cdot\boldsymbol{\nabla}\boldsymbol{U} - c_{\rm s}^2\boldsymbol{\nabla}\ln\rho + \boldsymbol{f} + \rho^{-1}\boldsymbol{\nabla}\cdot 2\rho\nu\mathbf{S}, \tag{52}$$

$$\frac{\partial \rho}{\partial t} = -\boldsymbol{\nabla}\cdot(\boldsymbol{U}\rho), \tag{53}$$

where $\boldsymbol{f}$ is a random forcing function consisting of circularly polarized plane waves with positive helicity and random direction and phase, $\mathbf{S}$ is the traceless rate-of-strain tensor. The length of the wavevector of the forcing function, $|\boldsymbol{k}_{\rm f}|$, is chosen to be in a narrow band around an average wavenumber $k_{\rm f}$. We adjust the strength of the forcing such that the flow remains clearly subsonic (mean Mach number is around 0.1). The details of the forcing function used in the present work can be found in Appendix A of Brandenburg & Subramanian (2005). For forced turbulence, we define $\mathrm{Re}_M = u_{\rm rms}/\eta k_{\rm f}$.

We consider a domain of size $L_x \times L_y \times L_z$. In all cases, we take $L_x = L_y = L_z = 2\pi/k_1$. The ratio $k_{\rm f}/k_1$ is referred to as the scale separation ratio. Our model is characterized by the choice of fluid and magnetic Reynolds numbers as well as the Péclet number, based here on the wavenumber $k_{\rm f}$. The magnetic Reynolds number was defined in Equation (51). The fluid Reynolds and Péclet numbers are defined analogously,

$$\mathrm{Re} = u_{\rm rms}/\nu k_{\rm f}, \quad \mathrm{Pe} = u_{\rm rms}/\kappa k_{\rm f}, \tag{54}$$

where the magnetic diffusivity η is replaced by the viscosity ν and the molecular diffusivity κ, respectively.

We present the results in a non-dimensional form by normalizing $\tilde{\kappa_{\rm t}}(\omega)$, analogously to earlier work (Brandenburg et al. 2008a), by

$$\tilde{\kappa_{\rm t0}} = \tau\overline{u_z^2} = \tfrac{1}{2}\tau u_{\rm rms}^2 \quad \text{(for the Roberts flow)}. \tag{55}$$

For turbulent flows, τ is proportional to the turnover time, $(u_{\rm rms}k_{\rm f})^{-1}$. However, in the limit of low Péclet number, microscopic diffusion becomes important and dominates over the triple correlation terms. This means that the effective τ is given by the microscopic diffusion time $\tau = (\kappa k_{\rm f}^2)^{-1}$.

We define the Strouhal number as $\mathrm{St} = \tau u_{\rm rms}k_{\rm f}$ and can then write τ as

$$\tau = \mathrm{St}/(u_{\rm rms}k_{\rm f}). \tag{56}$$

The value of St characterizes the flow field. For turbulent flows of the form discussed in the present paper, its value is of order unity (Brandenburg et al. 2004). Later in this paper we shall allow St to be a fit parameter. We present the results for α and $\eta_{\rm t}$by normalizing, depending on the nature of the flow with

$$\tilde{\alpha}_0 = -\tfrac{1}{2}u_{\rm rms}, \quad \tilde{\eta}_{\rm t0} = \tfrac{1}{2}u_{\rm rms}k_{\rm f}^{-1} \quad \text{(Roberts flow)} \tag{57}$$

and

$$\tilde{\alpha}_0 = -\tfrac{1}{3}u_{\rm rms}, \quad \tilde{\eta}_{\rm t0} = \tfrac{1}{3}u_{\rm rms}k_{\rm f}^{-1} \quad \text{(3D turbulence)}. \tag{58}$$

as was done in Brandenburg et al. (2008a).

6. RESULTS

Our choice of Equation (11) results in transport coefficients that depend on the wavenumber of the mean fields. Throughout this section, we will assume that our mean fields vary spatially according to $k_z = k_1$ unless otherwise specified. For simplicity, therefore, we drop the fixed argument k_z in $\tilde{\kappa}(k_z,\omega)$, $\tilde{\alpha}(k_z,\omega)$, and $\tilde{\eta}_{\rm t}(k_z,\omega)$, and similarly for $\tilde{\kappa}(k_z,s)$, $\tilde{\alpha}(k_z,s)$, and $\tilde{\eta}_{\rm t}(k_z,s)$.

6.1. Passive Scalar Diffusion

We now consider solutions of Equation (21) in the case of a turbulent flow, and consider first the case with a uniform gradient of $\overline{C}$. This means that $\overline{G}^{c0}$ is now constant in space, with $\overline{G}^{c0} = G_0(t)$. The resulting data agree well with the expression Equation (36), where τ is given by Equation (56) with $\mathrm{St} = 2.7$; see Figure 5. The fact that $\mathrm{St} > 1$ should not be too surprising, because such a result has been obtained earlier for this flow, where τ was estimated as the relaxation time in the τ approximation (Brandenburg et al. 2004).

The case of the Roberts flow where $\boldsymbol{U}$ is obtained from Equations (49) and (50) is in some ways more interesting. In the case of the same uniform gradient concentration $\overline{C}^{c0}$, the flux can be calculated analytically, as is done in Appendix B. As the flow $\boldsymbol{U}$ is steady, its correlation timescale is infinite and the only relevant relaxation timescale is the microscopic diffusion time $\tau = (\kappa k_{\rm f}^2)^{-1}$. The calculations result in the expression

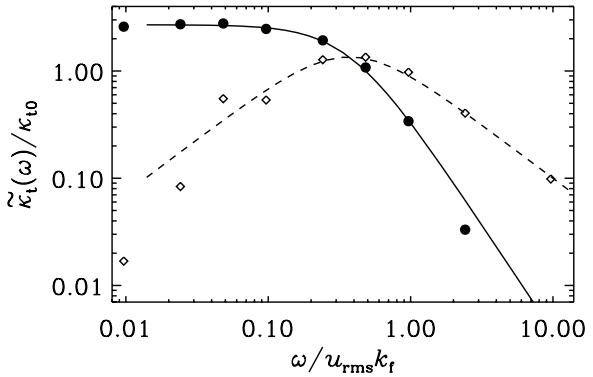

Figure 5. Real (solid circles) and imaginary (diamonds) parts of $\tilde{\kappa}(\omega)$ for forced turbulence with $k_f/k_1 = 2.2$, Re $= 8$, and Pe $= 40$. The solid and dashed lines are a fit using Equation (36) (with τ determined using Equation (56), St $= 2.7$ as described in text).

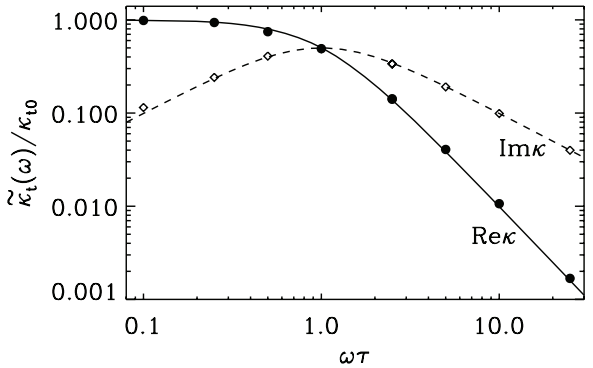

Figure 6. Real and imaginary parts of $\tilde{\kappa}(\omega)$ for Pe $= 100$ for the Roberts flow. Note the perfect agreement with the fit formula (Equation (36)) using $\tau = 1/(\kappa k_f^2)$ and $\kappa_{t0} = \tau u_{\rm rms}^2/2$ (curves).

$\tilde{\kappa}_t(\omega) = \kappa_{t0}/(1 - i\omega\tau)$; see Equation (36). This agrees with simulations as shown in Figure 6.

We suggested in Section 4.2 that advective effects play a role only when the mean concentration gradient shows a variation in some direction (i.e., a finite wavenumber), and we should not be surprised that Equation (36) is adequate to explain the transport of a passive scalar with zero wavenumber. The results of Figure 7, where a turbulent flow is used with Re $= 8$ and Pe $= 40$, and a sinusoidal variation of the mean concentration is imposed, are slightly better fitted with Equation (42) than with Equation (36).

The case of the flow $\boldsymbol{U} = u_0\hat{\boldsymbol{z}}\cos x$ with the same sinusoidally varying concentration is discussed in Appendix C. The value of ω where $\mathrm{Re}\,\tilde{\kappa}_t = \mathrm{Im}\,\tilde{\kappa}_t$ is not the same as the value of ω, where $\mathrm{Im}\,\tilde{\kappa}_t$ has zero slope. This is implied by Equation (36), as is discussed in Section 4.1. In Appendix C, we present a simple one-dimensional model where the behavior is at odds with Equation (36), although it can still be fitted reasonably well with Equation (42). This example also illustrates the difficulty in developing good and simple fits, as the fit parameters are expected to depend on the spatial variability (e.g., through $\omega_0 \sim ku$).

6.2. Magnetic Fields

For small magnetic Reynolds numbers the functional forms of both $\tilde{\alpha}(\omega)$ and $\tilde{\eta}_t(\omega)$ are similar to those in the passive scalar case. This is demonstrated here for the Roberts flow; see Figure 8, where $\mathrm{Re}_M = 1$, which is too small for dynamo action.

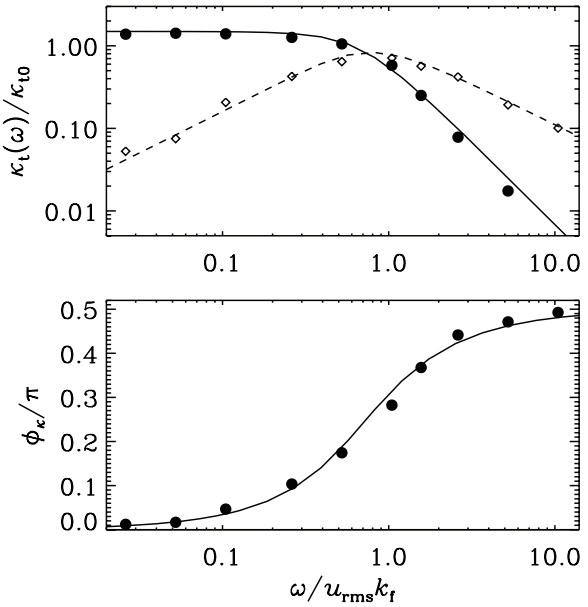

Figure 7. Real and imaginary parts of $\tilde{\kappa}(\omega)$ (upper panel) and its phase (lower panel) for turbulence at Re $= 8$ and Pe $= 40$. The solid and dashed lines are fits.

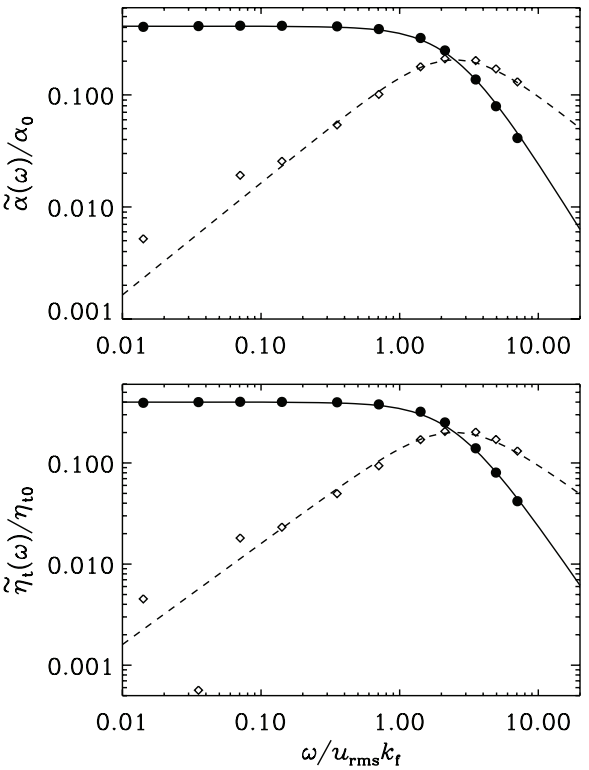

Figure 8. Real and imaginary parts of $\tilde{\alpha}(\omega)$ and $\tilde{\eta}_t(\omega)$ for the Roberts flow with $\mathrm{Re}_M = 1$. The solid and dashed lines correspond to fits of the form Equation (36) using Equation (56) with St $= 0.4$.

Figure 9 shows the s dependence for the same case. However, for $\mathrm{Re}_M = 10$, which is large enough for dynamo action, the forms of $\tilde{\alpha}(\omega)$ and $\tilde{\eta}_t(\omega)$ look rather different; see Figure 10, which is also for the Roberts flow. Qualitatively, the data are now closer to Equation (42), but a fit would be relatively poor. Therefore, we cannot rely on a fit to compute the corresponding Laplace-transformed kernel functions, which are shown in Figure 11 for $\mathrm{Re}_M = 10$ and 50. Note that, unlike the case of Figure 9 for

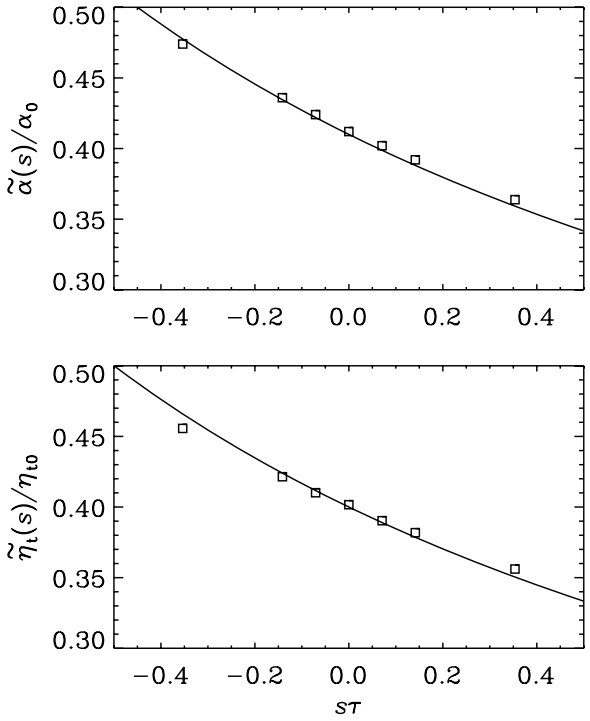

Figure 9. Similar to Figure 8, but for the Laplace-transformed kernel functions $\tilde{\alpha}(s)$ and $\tilde{\eta}_t(s)$ for the Roberts flow with $\mathrm{Re}_M = 1$. The fits are proportional to $\tau/(1+s\tau)$ and correspond to the fits used in Figure 8.

$\mathrm{Re}_M = 1$, for $\mathrm{Re}_M = 10$ and 50, the slope of $\hat{\alpha}(s)$ is positive. This is also a feature found by Hori & Yoshida (2008); see their Figure 10 for $\mathrm{Re}_M = 4$, which corresponds to $\mathrm{Re}_M = 8$ in our definition of the Roberts flow.

Figure 11 allows us now to assess the error done by applying the dispersion relation Equation (6) with constant values of α and η_t to cases where $\lambda \neq 0$. A correct procedure would be to use $\tilde{\alpha}(s)$ and $\tilde{\eta}_t(s)$ for $s = \lambda$. This means that we must calculate

$$\tilde{\lambda}(s) \equiv \tilde{\alpha}(s)k_z - [\eta + \tilde{\eta}_t(s)]k_z^2 \tag{59}$$

for $s = \lambda$. These points can be obtained from the intersection of $\lambda(s)$with the diagonal, $\lambda(s) = s$. For $\mathrm{Re}_M = 10$ and 50, these values are at $\lambda(s = \lambda) \approx 0.07 u_{\rm rms} k_{\rm f}$ and $\approx 0.11 u_{\rm rms} k_{\rm f}$, respectively. By contrast, $\lambda(s = 0) \approx 0.04 u_{\rm rms} k_{\rm f}$ and $\approx 0.07 u_{\rm rms} k_{\rm f}$ for these two values of Re_M, respectively. These values are now in full agreement with those of $\lambda_{\rm growth}$ seen in Figure 1. This suggests that the reason for the discrepancy between the two curves in this figure is indeed connected with memory effects.

Let us now turn to the calculation of $\tilde{\alpha}(\omega)$ and $\tilde{\eta}_t(\omega)$ in the case of turbulence. In this work, we use $k_{\rm f}/k_1 = 3$, which is slightly larger than the values used earlier in the case of a passive scalar. This value is just large enough to allow for mean-field dynamo action at the minimal wavenumber $k = k_1$ (see Brandenburg et al. 2008c). For $k_{\rm f}/k_1 = 2.2$, the scale separation between the scale of the forcing and that of the domain would be insufficient to allow for large-scale dynamo action (Haugen et al. 2004, Figure 23).

By comparing runs of two different magnetic Reynolds numbers, Figure 12 for $\mathrm{Re}_M = 22$ and Figure 13 for $\mathrm{Re}_M = 90$, we can get some idea whether the features seen here are artifacts of small values of Re_M, or whether they begin to be of more general significance. The plots for $\tilde{\alpha}(\omega)$ and $\tilde{\eta}_t(\omega)$ look similar and share the same basic features at both values of Re_M,

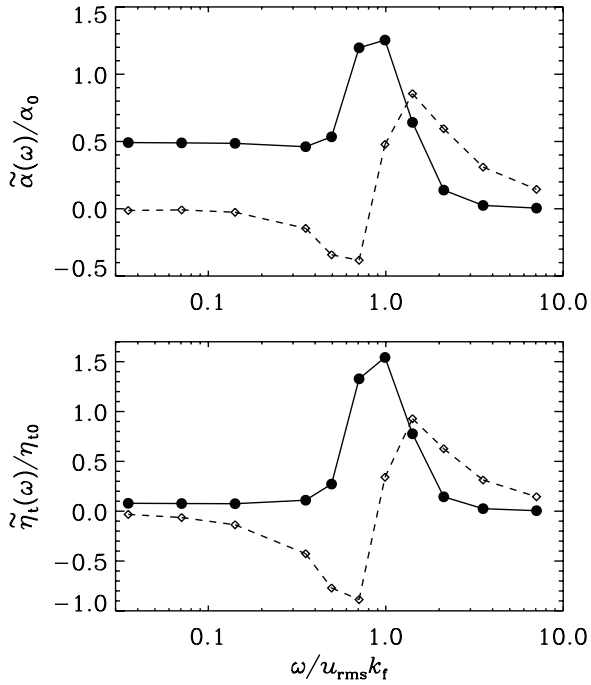

Figure 10. Real and imaginary parts of $\tilde{\alpha}(\omega)$ and $\tilde{\eta}_t(\omega)$ for the Roberts flow with $\mathrm{Re}_M = 10$. Note that the lines are not analytical fits.

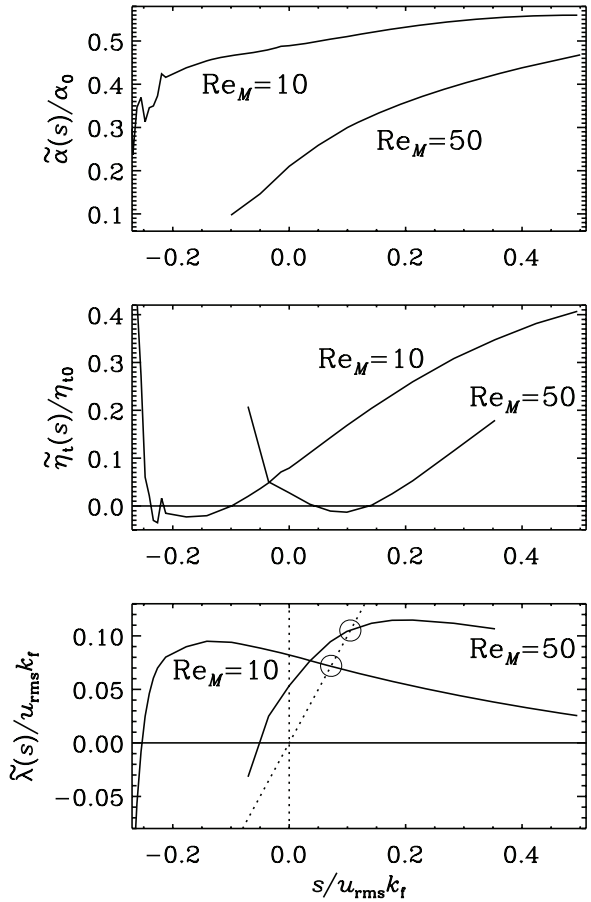

Figure 11. Laplace-transformed quantities, $\tilde{\alpha}(s)$, $\tilde{\eta}_t(s)$, and $\tilde{\lambda}(s)$ for the Roberts flow with $\mathrm{Re}_M = 10$ and 50. Note the different signs of the slope at the intersection with the diagonal (denoted by circles).

suggesting that the resulting fits for the response functions might be robust. We note that in all cases the phase shows a gradual transition from 0 to $\pi/2$ as ω increases, but it does not

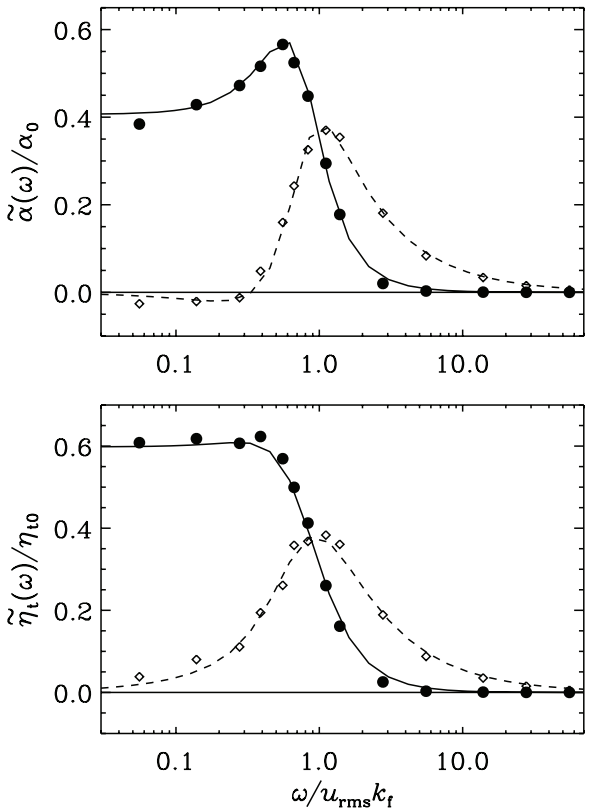

Figure 12. Real and imaginary parts of $\tilde{\alpha}(\omega)$ and $\tilde{\eta}_t(\omega)$ for turbulence at $\mathrm{Re}_M = 22$. The lines denote fits to Equations (44) and (45) with $A_\alpha = 1$, $\mathrm{St}_\alpha = 2.0$, $\omega_\alpha\tau_\alpha = 1.2$, and $A_\eta = 0.48$, $\mathrm{St}_\eta = 1.4$, $\omega_\eta\tau = 0.55$, respectively.

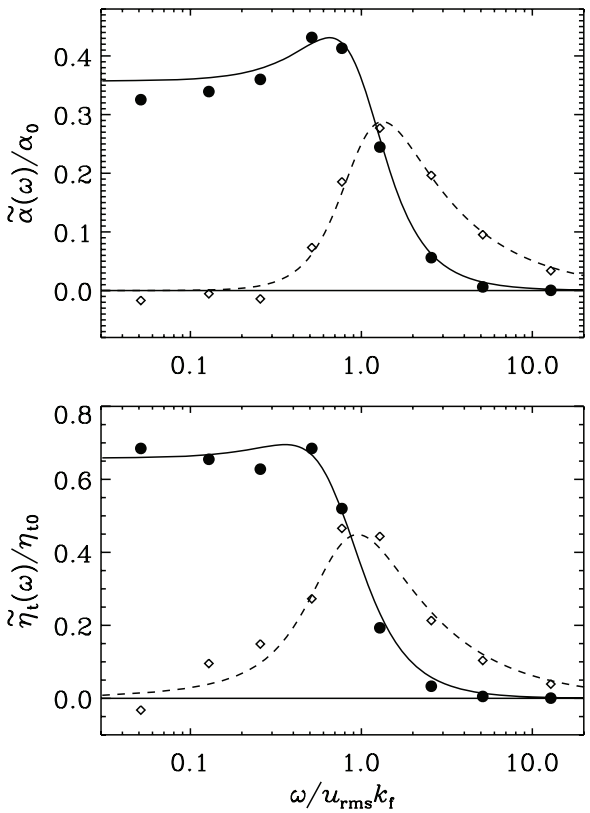

Figure 13. Real and imaginary parts of $\tilde{\alpha}(\omega)$ and $\tilde{\eta}_t(\omega)$ for turbulence at $\mathrm{Re}_M = 90$. The lines denote fits to Equations (44) and (45) with $A_\alpha = 1$, $\mathrm{St}_\alpha = 1.4$, $\omega_\alpha\tau_\alpha = 1$, and $A_\eta = 1.8$, $\mathrm{St}_\eta = 1.7$, $\omega_\eta\tau = 0.78$, respectively.

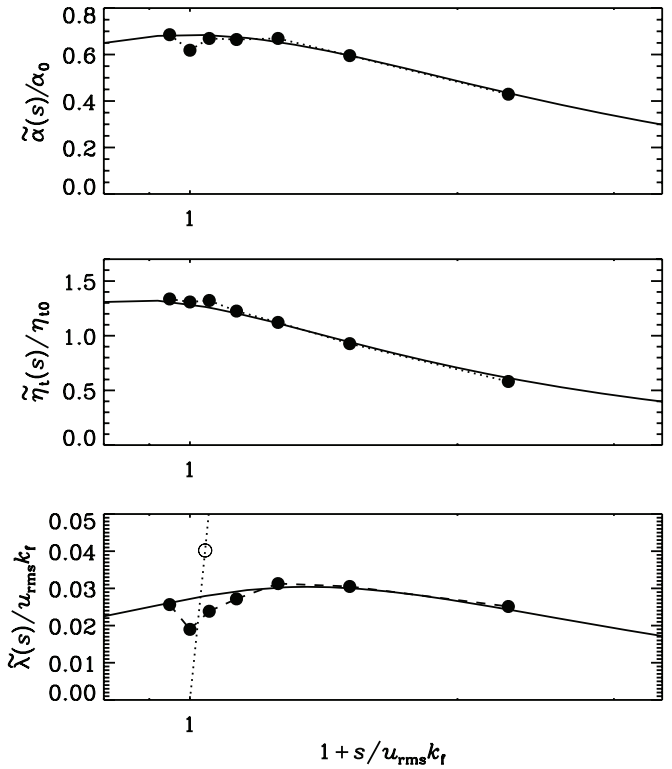

Figure 14. Laplace-transformed quantities, $\tilde{\alpha}(s)$, $\tilde{\eta}_t(s)$, and $\tilde{\lambda}(s)$ for forced turbulence at $\mathrm{Re}_M = 90$. In the last panel, the diagonal $\lambda = s$ is shown as a dotted line. The growth rate obtained by solving the three-dimensional induction equation, which allows for small-scale dynamo action, is indicated by an open symbol.

Table 1
Comparison of Fit Coefficients for $\tilde{\alpha}(\omega)$ and $\tilde{\eta}_t(\omega)$ for Forced Turbulence

Re	A_α	St_α	$\omega_\alpha\tau_\alpha$	A_η	St_η	$\omega_\eta\tau_\eta$
22	1.00	2.00	1.20	0.48	1.40	0.55
90	1.00	1.40	1.00	1.80	1.70	0.78

become negative (not shown). The corresponding fit parameters are summarized in Table 1. All the six non-dimensional fit parameters should be of order unity, and we see that this is indeed the case. Given that these values have unknown errors connected with the ambiguity in determining good fits, it is not possible to draw any serious conclusions from the trends that could be read off the table.

Similar to the case of the Roberts flow, the fits to the Fourier transformed quantities are not perfect. Therefore, we cannot use the Fourier transform fits to determine the corresponding Laplace transforms. In Figure 14, we show the directly determined Laplace-transformed values and compare with the fit inferred from Figure 13. However, in order to make the fits agree reasonably well, we have modified the amplitude factors to $A_\alpha = 1.37$ and $A_\eta = 2.07$. Note that the agreement is reasonably good, except near $s = 0$, where the actual growth rate is lower than what is inferred from the fit. This is related to the fact that the actual value of $\tilde{\alpha}(s)$ near $s = 0$ is less than what is predicted by the fit formula. This suggests that the assumption of similar fit formulae both for α and η_t may be too simplistic.

As for the Roberts flow, the actual growth rate of the mean-field dynamo is obtained from the intersection with the diagonal, which is shown as a dotted line in Figure 14. By solving the induction equation for this flow for $\mathrm{Re}_M = 90$, we find that the

actual growth rate is $0.04 u_{\rm rms} k_{\rm f}$, which is clearly above the point where $\lambda(s)$ intersects with the diagonal (see the open symbol). However, this is to be expected, because for $\mathrm{Re}_M = 90$ there is strong small-scale dynamo action so the actual growth rate will always exceed that expected from the mean-field dynamo. Such a discrepancy was noticed recently in connection with a study of the dependence of large-scale dynamo action on the magnetic Prandtl number (Brandenburg 2009).

7. DISCUSSION

7.1. Frequency and Growth Rate Dependence

An important application of the present results is the determination of dynamo growth rates. The usual dispersion relation for isotropic helical turbulence predicts the growth rate to be

$$\lambda = \alpha k - (\eta + \eta_{\rm t}) k^2 \quad \text{(for constant } \alpha, \eta_{\rm t}\text{)}. \tag{60}$$

However, if the resulting magnetic field really were to grow like $e^{\lambda t}$, the effective values of α and $\eta_{\rm t}$ would be modified and would no longer be constant. By applying Equations (44) and (45) for a range of values of λ for which $1 + \lambda\tau > 0$, we find that α and $\eta_{\rm t}$ become

$$\alpha(\lambda) = \alpha_0 A_\alpha \frac{1 + \lambda\tau_\alpha}{(1 + \lambda\tau_\alpha)^2 + \omega_\alpha^2 \tau_\alpha^2} \tag{61}$$

and

$$\eta_{\rm t}(\lambda) = \eta_{t0} A_{\eta_{\rm t}} \frac{1 + \lambda\tau_{\eta_{\rm t}}}{\left(1 + \lambda\tau_{\eta_{\rm t}}\right)^2 + \omega_{\eta_{\rm t}}^2 \tau_{\eta_{\rm t}}^2}, \tag{62}$$

respectively. In these equations, the occurrence of the terms $\omega_i \tau_i$ for $i = \alpha$ or $\eta_{\rm t}$ is qualitatively new compared with earlier expectations based on the τ approximation; see Section 4.1. Note that the relaxation times τ_i and oscillation frequency ω_i from Equation (41) are in general different for α and $\eta_{\rm t}$; see Table 1.

A more direct way of calculating $\alpha(\lambda)$ and $\eta_{\rm t}(\lambda)$ is by using exponentially growing or decaying test functions proportional to e^{st}, provided that $1 + s\tau > 0$, which sets the maximal decay rate for which Equations (61) and (62) are meaningful. The existence of a maximal decay rate is interesting: in such a system the fluctuating fields survive long enough to preserve the mean field. Clearly then, solutions of Equation (60)

$$\lambda = \alpha(\lambda) k - [\eta + \eta_{\rm t}(\lambda)] k^2 \tag{63}$$

are required for self-consistent systems (be they dynamos or decaying mean fields).

7.2. Wavenumber Dependence

In the work of Brandenburg et al. (2008a), which led to this paper, similar methods were used to find the dependences of α and $\eta_{\rm t}$ on the wavenumber k of the mean magnetic field. In that paper, it was shown for the Roberts flow that under FOSA we have

$$\tilde{\alpha}(k) = \frac{\alpha_0}{1 + (a_\alpha k/k_{\rm f})^2}, \qquad \tilde{\eta}_{\rm t}(k) = \frac{\eta_{\rm t0}}{1 + (a_\eta k/k_{\rm f})^2}, \tag{64}$$

where $a_\alpha = a_\eta = 1$. They found that this result is also a good approximation to turbulent flows, but then a_α and a_η were treated as fit parameters that are of order unity. While that work noted that memory effects should be expected, they were not treated. Equation (64) can be directly compared to Equation (61) with the growth rate λ set to 0 which recaptures the test-field method as used in Brandenburg et al. (2008a). This might suggest that $\cos\omega_0 t$ is related to the advection term in Equation (41), so one might expect that $\omega_0 \sim k u_{\rm rms}$. For $\omega_0 = \mathrm{St}_i k u_{\rm rms}$ then, the formulae from Equations (61) and (64) and match exactly, and by capturing the dependency of α and $\eta_{\rm t}$ on past times, we are perforce treating the problem as also non-local in space. One might therefore be tempted to suggest that the combined dependence on ω and k could be of the form

$$\tilde{\alpha}(k, \omega) = \alpha_0 A_\alpha \frac{1 - i\omega\tau_\alpha}{(1 - i\omega\tau_\alpha)^2 + (a_\alpha k/k_{\rm f})^2}, \tag{65}$$

and

$$\tilde{\eta}_{\rm t}(k, \omega) = \eta_{t0} A_{\eta_{\rm t}} \frac{1 - i\omega\tau_{\eta_{\rm t}}}{\left(1 - i\omega\tau_{\eta_{\rm t}}\right)^2 + (a_\eta k/k_{\rm f})^2}. \tag{66}$$

However, although such a formula is indeed obeyed in the two special cases $\omega = 0$ (Brandenburg et al. 2008a) and $k = k_1$ (present work), some preliminary work suggests that this equation is not valid in general, and that a multiplicative relation of the form $\tilde{\alpha}(k, \omega) = \tilde{\alpha}(k)\tilde{\alpha}(\omega)$ and $\tilde{\eta}_{\rm t}(k, \omega) = \tilde{\eta}_{\rm t}(k)\tilde{\eta}_{\rm t}(\omega)$ might be more accurate.

7.3. Linear Time Dependence

After our paper appeared in preprint form, Hughes & Proctor (2009) pointed out an inconsistency in the turbulent magnetic diffusivity tensor when allowing mean fields with a linear time dependence. They attributed this to the occurrence of a new contribution to the magnetic diffusivity. In the following, we explain that their result is a natural consequence of using Equations (44) and (45), as advocated in our paper.

The time dependence of the mean field in the paper by Hughes & Proctor (2009) is given by

$$\overline{\boldsymbol{B}}(t) = \boldsymbol{B}_0 + \boldsymbol{C}_0 t, \tag{67}$$

with constants $\boldsymbol{B}_0$ and $\boldsymbol{C}_0$. If we convolve this mean field with the kernels $\hat{\alpha}$ and $\hat{\eta}$, corresponding to the τ approximation (i.e., proportional to e^{-t/τ_α} and e^{-t/τ_η}, respectively), we find the $\overline{\boldsymbol{\mathcal{E}}}$ to be

$$\overline{\boldsymbol{\mathcal{E}}}(t) = (\alpha_0 - \eta_{\rm t0} k)(\boldsymbol{B}_0 + \boldsymbol{C}_0 t) - (\tau_\alpha \alpha_0 - \tau_\eta \eta_{\rm t0} k)\boldsymbol{C}_0. \tag{68}$$

This formulation matches the form of Equation (25) of Hughes & Proctor (2009), where their Γ is given by $-(\tau_\alpha \alpha_0 - \tau_\eta \eta_{\rm t0} k)$. Re-expressing Equation (68) in terms of $\overline{\boldsymbol{B}}(t)$ and $\partial\overline{\boldsymbol{B}}/\partial t$, as well as their curls, proportional $\overline{\boldsymbol{J}}(t)$ and $\partial\overline{\boldsymbol{J}}/\partial t$, we can write Equation (68) in the form

$$\overline{\boldsymbol{\mathcal{E}}} = \alpha_0 \overline{\boldsymbol{B}} - \eta_{\rm t0}\mu_0 \overline{\boldsymbol{J}} + \Gamma_\alpha \frac{\partial \overline{\boldsymbol{B}}}{\partial t} - \Gamma_\eta \mu_0 \frac{\partial \overline{\boldsymbol{J}}}{\partial t}, \tag{69}$$

where $\Gamma_\alpha = -\alpha_0 \tau_\alpha$ and $\Gamma_\eta = -\eta_{\rm t0} \tau_\eta$ quantify additional contributions to the mean electromotive force. In the more general case, where ω_α and ω_η are different from zero, we have

$$\Gamma_\alpha = -\alpha_0 \tau_\alpha \frac{1 - \omega_\alpha^2 \tau_\alpha^2}{\left(1 + \omega_\alpha^2 \tau_\alpha^2\right)^2}, \quad \Gamma_\eta = -\eta_0 \tau_\eta \frac{1 - \omega_\eta^2 \tau_\eta^2}{\left(1 + \omega_\eta^2 \tau_\eta^2\right)^2}. \tag{70}$$

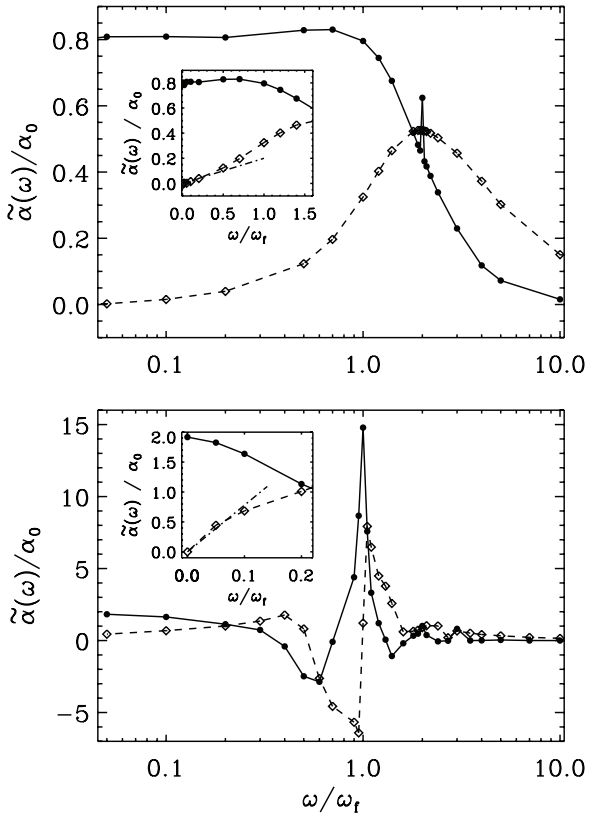

Figure 15. Real and imaginary parts of $\tilde{\alpha}(\omega)$ for $k = 0$ using the Otani (1993) MW+ flow with $\mathrm{Re}_M = 1$ (upper panel) and $\mathrm{Re}_M = 100$ (lower panel). The normalization is chosen to be $\alpha_0 = u_0$. The insets show the scaling of $\mathrm{Im}\,\tilde{\omega}$ near the origin with slopes 0.2 and 7.8 for the upper and lower panels, in agreement with the results of Hughes & Proctor (2009).

We recall that the formulation in Equation (69) only applies to the special case of variations of the mean field that are linear in time. More generally, we have

$$\overline{\mathcal{E}} = \sum_{n=0}^{\infty}(-1)^n\left(\alpha^{(n)}\frac{\partial^n\overline{\boldsymbol{B}}}{\partial t^n} - \eta^{(n)}\mu_0\frac{\partial^n\overline{\boldsymbol{J}}}{\partial t^n}\right), \tag{71}$$

where

$$\alpha^{(n)} = \int_0^\infty \hat{\alpha}(t)\,t^n\,\mathrm{d}t, \qquad \eta_{\rm t}^{(n)} = \int_0^\infty \hat{\eta}(t)\,t^n\,\mathrm{d}t. \tag{72}$$

These moments are related to the derivatives of $\tilde{\alpha}(\omega)$ and $\tilde{\eta}_{\rm t}(\omega)$ at $\omega = 0$ with

$$\alpha^{(n)} = (-i)^n\left.\frac{\mathrm{d}^n\tilde{\alpha}}{\mathrm{d}\omega^n}\right|_0, \qquad \eta_{\rm t}^{(n)} = (-i)^n\left.\frac{\mathrm{d}^n\tilde{\eta}}{\mathrm{d}\omega^n}\right|_0, \tag{73}$$

where the subscripts 0 indicate that the derivatives are to be evaluated at $\omega = 0$. Note, in particular, that $\Gamma_\alpha = -\alpha^{(1)} = \mathrm{Im}(\mathrm{d}\tilde{\alpha}/\mathrm{d}\omega)_0$.

Hughes & Proctor (2009) have computed values of Γ_α for Re_M between 1 and 100 using a particular form of the modulated wave flow of Otani (1993), referred to as MW+ flow, which is given by Equation (49) with $k_{\rm f} = k_0$ and

$$\psi(x, y, t) = \frac{2u_0}{k_0}(\cos^2\omega_{\rm f}t\cos k_0x - \sin^2\omega_{\rm f}t\cos k_0y), \tag{74}$$

where $\omega_{\rm f} = u_0k_0$ has been chosen.

In order to substantiate our interpretation of their results, we have computed $\tilde{\alpha}(\omega)$ for their case with $k = 0$. The result for the Fourier-transformed kernel is shown in Figure 15 for the Otani MW+ flow with $\mathrm{Re}_M = 1$ and 100. Compared with Figure 3, there are additional features related to resonances with the frequency $\omega_{\rm f}$ of the Otani flow. Such features cannot be explained with our simple fit formula. This means that higher order terms will become important in those cases where the variation of the mean magnetic field is more complicated than just a linear increase.

The value of Γ_α can readily be read off as the slope of the graph of $\mathrm{Im}\,\tilde{\omega}$ near the origin. Our results agree with those of Hughes & Proctor (2009), as is shown in the insets of Figure 15. We note, however, there are no good reasons to associate the Γ_α term with a correction to turbulent diffusion alone. Instead, there are corrections both to α and to $\eta_{\rm t}$ once the mean magnetic field shows strong time dependence.

In this connection, it is important to emphasize that these complications are mainly a consequence of the particular time dependence inherent to the Otani flow and are not typical of turbulence, as seen before. For $\mathrm{Re}_M = 100$ there is a distinct spike at $\omega = \omega_{\rm f}$, while for $\mathrm{Re}_M = 1$ there is a smaller spike at $\omega = 2\omega_{\rm f}$; see Figure 15. We hypothesize that these spikes are associated with the periodicity of the Otani flow. Similar behavior is known to occur for the Galloway & Proctor (1992) flow (Courvoisier et al. 2006), and is connected with the infinite correlation time of a flow with sinusoidal time dependence (Rädler & Brandenburg 2009).

8. CONCLUSIONS

Naive application of the values of α and $\eta_{\rm t}$ to time-dependent problems can lead to errors. This is because the turbulent transport coefficients are in general frequency-dependent, due to memory effects. So, for each frequency and for each growth or decay rate (corresponding to imaginary frequencies) the transport coefficients need to be determined separately. The full frequency dependence can then be used to calculate response functions via Fourier transformation. The result can then be used to determine the response to general time dependences, including, for example, oscillatory growth.

The response function formalism shows that one needs to know the past time history of the mean fields to compute turbulent transport correctly. This is not new, but what is new is the fact that the departures from the instantaneous approximation can be quite substantial for flows such as the Roberts flow. For isotropic turbulence, on the other hand, the effects tend to be less dramatic and simple fit formulae with an exponential decay and an oscillatory part can be reasonably accurate.

The presence of an oscillatory part in the response function proportional to $\cos\omega_0t$ leads to a sign reversal of α and $\eta_{\rm t}$. Hori & Yoshida (2008) associate this with the "over-twisting" in illustrations of Parker's Ω loops. In their picture, rising flux tubes may twist by more than 90°. This interpretation clarifies the naive expectation that α may change the sign when the Coriolis force becomes important. In fact, as our work now shows, such an effect would only occur if the mean magnetic field varies like a δ function in time or if it shows other rapid variations. Conversely, for mean fields varying slowly in time the net α would not change sign, although some past times are weighted negatively.

In the present work, we have only looked at one type of memory effect, where the typical timescales in the integral

kernel are comparable to the dynamical timescales of the turbulence. There is yet another type of memory effect that can occur on a resistive timescale, namely the one associated with magnetic helicity conservation. As explained in the appendix of Blackman & Brandenburg (2002), this is a purely nonlinear effect such that the relevant timescale becomes very long only when the magnetic field is strong. Obviously, this effect is not captured by our kinematic approach, nor would it be relevant in connection with the calculation of growth rates of the dynamo.

The approach presented here may be useful for calculating memory effects of turbulent transport coefficients over a range of other related problems. Particularly important might be the question of the damping of acoustic waves by turbulent viscosity in the Sun, for example (Stix et al. 1993). Such damping would lead to line broadening of the acoustic frequencies. The present work has demonstrated that such quantities can only be useful if one has a good idea of its frequency dependence relative to the frequency at which the turbulent viscosity is determined and the frequency at which it is to be applied.

Our approach could also be useful in cases where the turbulence itself is time dependent. This would be relevant for modeling convection in pulsating stars. Such systems are currently being treated with time-dependent mixing length theory (Gough 1977). It would seem appropriate to adopt integral kernels also in that case. However, now there would be two frequencies to be considered: the frequency at which the turbulence varies and the frequency at which the mean field varies. Another problem is that the test-field method has only been used and tested in connection with magnetic and passive scalar diffusion problems, and has not yet been developed for calculating the components of the turbulent viscosity tensor. This would indeed be one of the outstanding problems in this field.

We thank the referee for suggesting many improvements to the paper and for presenting us with the calculation that is now reproduced in Appendix B. We acknowledge Matthias Rheinhardt for making useful suggestions. The computations have been carried out on the National Supercomputer Centre in Linköping and the Center for Parallel Computers at the Royal Institute of Technology in Sweden. This work was supported in part by the Swedish Research Council, grant 621-2007-4064, and the European Research Council under the AstroDyn Research Project 227952.

APPENDIX A

CONVOLUTION FOR MONOCHROMATIC VARIATIONS

The purpose of this appendix is to show that for monochromatic signals a convolution corresponds to a multiplication in real space. Consider Equation (A1) for a monochromatic function

$$\overline{\boldsymbol{G}}(t)=\overline{\boldsymbol{G}}_\omega(t)\equiv\boldsymbol{G}_0\cos\omega t, \tag{A1}$$

where ω is a constant. Inserting this into Equation (12) yields

$$\begin{aligned}\overline{\mathcal{F}}_\omega(t)&=-\int_{-\infty}^{\infty}\hat{\kappa}_{\rm t}(t-t')\boldsymbol{G}_0\cos\omega t'\,{\rm d}t'\\&=-\boldsymbol{G}_0{\rm Re}\int_{-\infty}^{\infty}\hat{\kappa}_{\rm t}(t-t')e^{-i\omega t'}\,{\rm d}t'\\&=-\boldsymbol{G}_0{\rm Re}\,e^{-i\omega t}\int_{-\infty}^{\infty}\hat{\kappa}_{\rm t}(t-t')e^{i\omega(t-t')}\,{\rm d}t'.\end{aligned} \tag{A2}$$

By using a change of variables one sees that the integral is just the Fourier transform of $\hat{\kappa}_{\rm t}(t)$. Thus, we arrive at

$$\overline{\mathcal{F}}_\omega(t)=-\boldsymbol{G}_0{\rm Re}[e^{-i\omega t}\tilde{\kappa}_{\rm t}(\omega)]. \tag{A3}$$

The real part of $\tilde{\kappa}_{\rm t}$ shows therefore a modulation with $\cos\omega t$ and the imaginary part with $\sin\omega t$. By projecting against these two functions separately, we can determine the real and imaginary parts of $\tilde{\kappa}(\omega)$. Thus, the complex function $\tilde{\kappa}(\omega)$ can be obtained from $\overline{\mathcal{F}}_\omega(t)$ as

$$\tilde{\kappa}_{\rm t}(\omega)=-2G_0^{-1}\langle e^{i\omega t}\overline{\mathcal{F}}_\omega(t)\rangle_t, \tag{A4}$$

which is the result stated in Equation (30). The factor 2 stems from the fact that the average values of $\cos^2\omega t$ and $\sin^2\omega t$ are $1/2$. This procedure can be trivially extended to tensorial relationships; cf. Equation (33).

It is interesting to write Equation (A3) by expressing $\tilde{\kappa}_{\rm t}(\omega)$ in terms of its modulus and its phase, $|\tilde{\kappa}_{\rm t}|\exp i\phi_\kappa$, so we have

$$\overline{\mathcal{F}}_\omega(t)=-|\tilde{\kappa}|\,\overline{G}(t-\Delta t),\qquad\text{where}\quad\Delta t=\phi_\kappa(\omega)/\omega, \tag{A5}$$

showing that memory effects change not only the amplitude of the effective transport coefficient, but they also lead to a time lag such that, for a given frequency, the mean flux is proportional to the mean fields at a certain later time.

APPENDIX B

ROBERTS FLOW WITH OSCILLATORY MEAN CONCENTRATION GRADIENT

As was generously pointed out by the referee, in the special case of a Roberts flow, Equations (49) and (50), with a mean concentration $\overline{C}=zG_0\cos\omega t$, we can solve the problem analytically. In this case, Equation (21) becomes

$$\frac{\partial c}{\partial t}=-u_zG_0\cos\omega t-\boldsymbol{\nabla}\cdot(\boldsymbol{u}c-\overline{\boldsymbol{u}c})+\kappa\nabla^2c. \tag{B1}$$

In a first step, we employ FOSA and neglect $\boldsymbol{\nabla}\cdot(\boldsymbol{u}c-\overline{\boldsymbol{u}c})$, so the above reduces to

$$\frac{\partial c}{\partial t}-\kappa\nabla^2c=-\sqrt{2}u_0G_0\cos k_0x\cos k_0y\cos\omega t. \tag{B2}$$

This has as a solution

$$c(x,y,t)=-\frac{\sqrt{2}u_0G_0}{\left(\omega^2+\left(\kappa k_{\rm f}^2\right)^2\right)^{1/2}}\cos k_0x\cos k_0y\cos(\omega t-\phi), \tag{B3}$$

where

$$\cos\phi=\frac{\kappa k_{\rm f}^2}{\left(\omega^2+\left(\kappa k_{\rm f}^2\right)^2\right)^{1/2}},\quad\sin\phi=\frac{\omega}{\left(\omega^2+\left(\kappa k_{\rm f}^2\right)^2\right)^{1/2}}. \tag{B4}$$

Note that $\boldsymbol{\nabla}\cdot(\boldsymbol{u}c-\overline{\boldsymbol{u}c})=0$ and so this particular solution is also valid beyond FOSA. We obtain then

$$\overline{\boldsymbol{\mathcal{F}}}^\omega(t)=-\frac{u_0^2G_0}{2\left(\omega^2+\left(\kappa k_{\rm f}^2\right)^2\right)^{1/2}}\cos(\omega t-\phi)\hat{\boldsymbol{z}}. \tag{B5}$$

We can now find the Fourier-transformed kernel through Equation (A4):

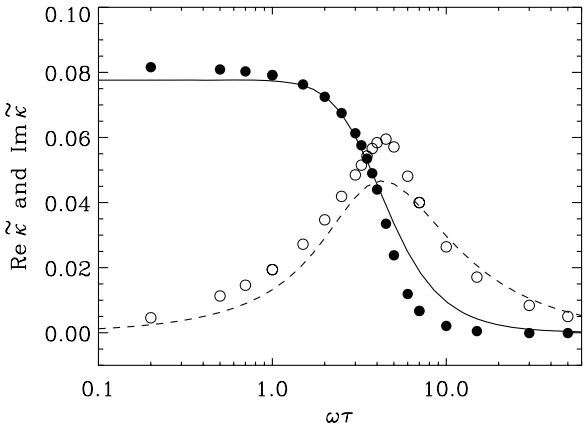

Figure 16. Real (solid circles) and imaginary (open circles) components of κ_t for $k_z = 5$ and $\boldsymbol{u} = u_0\hat{\boldsymbol{z}}\cos x$ (see Appendix C), using as fit parameters $A_\kappa = 0.105$, $\tau_\alpha = 0.33$, and $\omega_\kappa = 1.8$.

$$\begin{aligned}\tilde{\kappa_t}(\omega) &= -2G_0^{-1}\langle e^{i\omega t}\overline{\mathcal{F}}_\omega(t)\rangle_t \\ &= \frac{u_0^2}{2\left(\omega^2+\left(\kappa k_f^2\right)^2\right)^{1/2}}\left(\frac{\kappa k_f^2+i\omega}{\left(\omega^2+\left(\kappa k_f^2\right)^2\right)^{1/2}}\right) \\ &= \frac{\tau_k u_0^2}{2}\left(\frac{1+i\omega\tau_k}{1+\omega^2\tau_k^2}\right) = \frac{\tau_k u_0^2}{2}\left(\frac{1}{1-i\omega\tau_k}\right), \quad \text{(B6)}\end{aligned}$$

where we have defined $\tau_k^{-1} = \kappa k_f^2$. Equations (49) and (50) imply that $\overline{u_z^2} = u_0^2/2$, and Section 6.1 argues that $\tau = \tau_k$. Accordingly, Equation (B6) reduces to Equation (36).

APPENDIX C

SIMPLIFIED ONE-DIMENSIONAL MODEL

A simple system that defies result (Equation (36)) of the τ approximation is one with a passive scalar whose concentration varies sinusoidally along z with $k_z \neq 0$ and a steady flow $\boldsymbol{u} = (0, 0, u)$, such that $u = u(x) = u_0 \cos k_0 x$, so $\boldsymbol{\nabla}\cdot\boldsymbol{u} = 0$. The equation for the small-scale concentration then is

$$\frac{\partial c}{\partial t} = -\boldsymbol{\nabla}\cdot(\boldsymbol{u}\overline{C} + \boldsymbol{u}c - \overline{\boldsymbol{u}c}) + \kappa\nabla^2 c, \quad \text{(C1)}$$

which becomes

$$\frac{\partial c}{\partial t} = -u\overline{G} - u\frac{\partial c}{\partial z} + u\overline{\frac{\partial c}{\partial z}} + \kappa\nabla^2 c, \quad \text{(C2)}$$

and in turn

$$\frac{\partial c}{\partial t} = -u\frac{\partial c}{\partial z} + u\overline{\frac{\partial c}{\partial z}} + \kappa\nabla^2 c - u(x)\overline{G}(t, z). \quad \text{(C3)}$$

This system is linear, inhomogeneous, with variable coefficients. We note that $\overline{G}(t, z) = G(t)e^{ik_z z}$, impose

$$G(t) = G_0\cos\omega t, \quad \text{(C4)}$$

assume that

$$c = \tilde{c}(t, x)e^{ik_z z} + \text{c.c.} \quad \text{(C5)}$$

and treat as the system as a time-dependent problem with complex $\tilde{c}(t, x)$:

$$\frac{\partial\tilde{c}}{\partial t} = -\left[ik_z u(x) + \kappa k_z^2\right]\tilde{c} + \kappa\frac{\partial^2\tilde{c}}{\partial x^2} + ik_z\overline{u\tilde{c}} - u_0 G_0\cos k_0 x\cos\omega t. \quad \text{(C6)}$$

Equation (C6) is the equivalent equation to Equation (B2) (and reduces to that equation when $k_z = 0$). The Fourier-transformed kernel can be calculated similar to Appendix B, and in Figure 16 we present a numerical solution for the Fourier-transformed kernel for $k_z/k_1 = 5$ and $u_0/\kappa k_z = 5$.

REFERENCES

Blackman, E. G., & Brandenburg, A. 2002, ApJ, 579, 359
Blackman, E. G., & Field, G. B. 2002, Phys. Rev. Lett., 89, 265007
Blackman, E. G., & Field, G. B. 2003, Phys. Fluids, 15, L73
Blackman, E. G., & Field, G. B. 2004, Phys. Plasmas, 11, 3264
Brandenburg, A. 2001, ApJ, 550, 824
Brandenburg, A. 2009, ApJ, 697, 1153
Brandenburg, A., Käpylä, P., & Mohammed, A. 2004, Phys. Fluids, 16, 1020
Brandenburg, A., Rädler, K.-H., & Schrinner, M. 2008a, A&A, 482, 739
Brandenburg, A., Rädler, K.-H., Rheinhardt, M., & Käpylä, P. J. 2008b, ApJ, 676, 740
Brandenburg, A., Rädler, K.-H., Rheinhardt, M., & Subramanian, K. 2008c, ApJ, 687, L49
Brandenburg, A., & Subramanian, K. 2005, A&A, 439, 835
Brandenburg, A., Svedin, A., & Vasil, G. M. 2009, MNRAS, 395, 1599
Courvoisier, A. 2008, Geophys. Astrophys. Fluid Dyn., 102, 217
Courvoisier, A., Hughes, D. W., & Tobias, S. M. 2006, Phys. Rev. Lett., 96, 034503
Fedotov, S., Ivanov, A., & Zubarev, A. 2002, Phys. Rev. E, 65, 036313
Fedotov, S., Ivanov, A., & Zubarev, A. 2003, Geophys. Astrophys. Fluid Dyn., 97, 135
Galloway, D. J., & Proctor, M. R. E. 1992, Nature, 356, 691
Gough, D. O. 1977, ApJ, 214, 196
Haugen, N. E. L., Brandenburg, A., & Dobler, W. 2004, Phys. Rev. E, 70, 016308
Hori, K., & Yoshida, S. 2008, Geophys. Astrophys. Fluid Dyn., 102, 601
Hughes, D. W., & Proctor, M. R. E. 2009, arXiv:0906.2751
Kleeorin, N., Mond, M., & Rogachevskii, I. 1996, A&A, 307, 293
Krause, F., & Rädler, K.-H. 1980, Mean-Field Magnetohydrodynamics and Dynamo Theory (Oxford: Pergamon Press)
Moffatt, H. K. 1978, Magnetic Field Generation in Electrically Conducting Fluids (Cambridge: Cambridge Univ. Press), 175
Otani, N. F. 1993, J. Fluid Mech., 253, 327
Otmianowska-Mazur, K., Rüdiger, G., Elstner, D., & Arlt, R. 1997, Geophys. Astrophys. Fluid Dyn., 86, 229
Plunian, F., & Rädler, K.-H. 2002a, Geophys. Astrophys. Fluid Dyn., 96, 115
Plunian, F., & Rädler, K.-H. 2002b, Magnetohydrodynamics, 38, 92
Plunian, F., Marty, P., & Alemany, A. 1999, J. Fluid Mech., 382, 137
Rädler, K.-H., & Brandenburg, A. 2009, MNRAS, 393, 113
Rädler, K.-H., Rheinhardt, M., Apstein, E., & Fuchs, H. 2002, Nonl. Processes Geophys., 38, 171
Roberts, G. O. 1972, Phil. Trans. R. Soc. A, 271, 411
Schrinner, M., Rädler, K.-H., Schmitt, D., Rheinhardt, M., & Christensen, U. 2005, Astron. Nachr., 326, 245
Schrinner, M., Rädler, K.-H., Schmitt, D., Rheinhardt, M., & Christensen, U. R. 2007, Geophys. Astrophys. Fluid Dyn., 101, 81
Soward, A. M. 1987, J. Fluid Mech., 180, 267
Stieglitz, R., & Müller, U. 2001, Phys. Fluids, 13, 561
Stix, M., Rüdiger, G., Knölker, M., & Grabowski, U. 1993, A&A, 272, 340
Sur, S., Brandenburg, A., & Subramanian, K. 2008, MNRAS, 385, L15
Vainshtein, S. I., & Kitchatinov, L. L. 1983, Geophys. Astrophys. Fluid Dyn., 24, 273